

# QCD Thermodynamics from the Lattice

C.E. DeTar

*Physics Department, University of Utah, Salt Lake City, UT 84112, USA*

U.M. Heller

*American Physical Society, One Research Road, Ridge, NY 11961, USA*

(Dated: October 24, 2018)

## Abstract

We review the current methods and results of lattice simulations of quantum chromodynamics at nonzero temperatures and densities. The review is intended to introduce the subject to interested nonspecialists and beginners. It includes a brief overview of lattice gauge theory, a discussion of the determination of the crossover temperature, the QCD phase diagram at zero and nonzero densities, the equation of state, some in-medium properties of hadrons including charmonium, and some plasma transport coefficients.

PACS numbers:

## I. INTRODUCTION

Quantum chromodynamics is the well-established theory of interacting quarks and gluons. Although its Lagrangian is simple and elegant, except for high energy processes where perturbation theory is applicable, it is very difficult to solve. Over the past three decades *ab initio* numerical and computational methods have been devised for obtaining nonperturbative solutions. They have become refined to the point that a few dozen calculated quantities (decay constants, mass splittings, etc.) agree with known experimental values to a precision of a couple percent [1]. These successes provide the opportunity to push the calculations with some confidence into new regimes that have not been thoroughly explored experimentally. In this review we will be interested in numerical simulations of strongly interacting matter under the extreme conditions of high temperatures and/or high baryon number densities.

Shortly after the big bang the universe was very likely dominated by a high temperature plasma of quarks, antiquarks, and gluons. As the universe expanded and cooled, hadrons emerged that make up today's universe. Knowing the characteristics of the plasma and the nature of the transition to hadrons is clearly important for understanding these stages in the development of the universe. In the cores of some dense stars it is conceivable that the baryon number density is sufficiently high that hadrons lose their identities and merge into a plasma of quarks and gluons. The equation of state of such a dense plasma, for example, is important for understanding conditions leading to a collapse to a black hole. In heavy ion collisions at RHIC, FAIR, and soon at the LHC we seek to produce a quark-gluon plasma and study its properties. Since so little is known about the plasma, we turn to numerical simulation of high-temperature and moderate-density QCD to predict its properties and to guide the experimental investigation. Apart from the phenomenological interest in such simulations, there is also intrinsic theoretical interest in understanding the behavior of confining field theories under extreme conditions. In particular, there are tantalizing predictions of still new states of matter at very high densities [2]. Lattice QCD thermodynamics is understandably a popular and vigorous field of research.

Certainly, present day lattice simulations can't answer all of our questions. The current standard methodology assumes thermal equilibrium. Moreover, simulations at nonzero densities are still in their infancy, so much of what we know is restricted to zero or very small baryon number densities. To apply lattice results to the phenomenology of heavy ion collisions requires an intermediate model, such as hydrodynamics, which takes input from lattice simulations, adds model

assumptions, and makes predictions about the rapidly evolving, emerging matter. For this purpose the most important quantities obtained from lattice simulations are the phase diagram as a function of temperature and baryon number density, the equation of state, speed of sound, and transport properties, such as the viscosities and thermal conductivity.

In this review, intended for nonspecialists and beginners, we give a brief overview of the lattice methodology and discuss a variety of numerical results. We discuss challenges and potential sources of systematic error. In Sec. II we give a brief introduction to lattice gauge theory and discuss the advantages and disadvantages of various fermion formulations. We discuss a variety of observables used to determine the transition temperature  $T_c$  in Sec. III and comment on some disparate results. In Sec. IV we review our current understanding of the phase diagram at zero baryon density, and in Sec. V we do the same for nonzero baryon number densities. We discuss the variety of methods in current use for simulating at nonzero densities. We review the equation of state in Sec. VI. In Sec. VII we discuss some properties of hadrons in the high temperature medium, and in Sec. VIII some results for transport coefficients. Finally, in Sec. IX we summarize briefly the current state of the field, list outstanding problems, and list some prospects for resolving them.

## II. THERMODYNAMICS IN LATTICE GAUGE THEORY

### A. Quantum partition function

Quantum thermodynamics at a fixed, large volume is based on the partition function in the quantum canonical ensemble

$$Z = \text{Tr}[\exp(-H/T)], \tag{1}$$

where  $H$  is the quantum Hamiltonian operator,  $T$  is the temperature, and the trace is taken over the physical Hilbert space. At nonzero densities the grand canonical ensemble is appropriate:

$$Z = \text{Tr} \left[ \exp \left( -H/T + \sum_i \mu_i N_i/T \right) \right], \tag{2}$$

where  $\mu_i$  is the chemical potential for the  $i$ th species and  $N_i$  is the corresponding conserved flavor number. For example, in QCD we may introduce a separate chemical potential for each quark flavor. Zero chemical potential for a given flavor implies equal numbers of quarks and antiquarks of that flavor, so zero baryon number density, zero strangeness, etc.

The expectation value of an observable  $O$  at temperature  $T$  is computed with respect to this ensemble through

$$\langle O \rangle = \text{Tr} \left[ O \exp \left( -H/T + \sum_i \mu_i N_i / T \right) \right] / Z. \quad (3)$$

### B. Feynman path integral partition function

The Feynman path integral formalism provides a practical basis for the computation of thermodynamic quantities, especially in quantum field theory, where there are many degrees of freedom. It converts the trace over quantum states into a multidimensional integration over classical variables [3]. It is beyond the scope of this review to give a detailed derivation of the path integral formulation, particularly for a gauge theory with fermion fields. There are standard references [4, 5, 6].

The classical variables in the Feynman path integral are the path “histories” of the fundamental fields in Euclidean (imaginary) time  $\tau$ . (Imaginary, because the Boltzmann weight factor  $\exp(-H/T)$  is, in effect, a time evolution operator  $\exp(-iHt)$  for an imaginary time  $-i/T$ .) For computational purposes the histories are discretized in  $\tau$ . The quantum fields at any given time are also discretized in three-dimensional coordinate space  $\mathbf{x}$ . The resulting path integral is then a multidimensional integral over variables defined on a four-dimensional space-time lattice ( $x = \mathbf{x}, \tau$ ). The discretization of space and time introduces an error, but the error vanishes as the lattice spacing is taken to zero (continuum limit).

### C. Scalar field example

For a concrete example, consider a scalar field theory described by the Lagrange density

$$L(\phi) = \frac{1}{2} \sum_{\mu} \left[ \frac{\partial}{\partial x_{\mu}} \phi(x) \right]^2 + V[\phi(x)], \quad (4)$$

where  $V$  describes the mass and self-interaction. On a hypercubic lattice with point separation  $a$  and a central-difference discretization of the derivatives, we can write a lattice approximation

$$L[\phi(x)] = \frac{1}{8a^2} \sum_{\mu} [\phi(x + a\hat{\mu}) - \phi(x - a\hat{\mu})]^2 + V[\phi(x)]. \quad (5)$$

where  $\hat{\mu}$  is a unit coordinate vector in the  $\mu$  direction. A Euclidean time history is then specified simply by giving the values of the field  $\phi(\mathbf{x}, \tau)$  on all the lattice points  $(\mathbf{x}, \tau)$ . Each such history

corresponds to a classical Euclidean action  $S(\phi)$ , which is computed by summing its Lagrange density over the lattice points

$$S(\phi) = \sum_{\mathbf{x}, \tau} L[\phi(\mathbf{x}, \tau)]. \quad (6)$$

The partition function then becomes a multidimensional integral over the values of the field  $\phi(\mathbf{x}, \tau)$  at each point, weighted by the exponential of the classical Euclidean action:

$$Z = \int \prod_{\mathbf{x}, \tau} d\phi(\mathbf{x}, \tau) \exp[-S(\phi)]. \quad (7)$$

Two important conditions on the Euclidean time history are inherited from the definition [Eq. (1)] of the partition function: First, the time history  $\tau$  ranges over a finite interval from 0 to  $a(N_\tau - 1)$  where

$$1/T = aN_\tau, \quad (8)$$

which establishes the relation between the temperature and the Euclidean time extent of the lattice. Second, to reproduce the trace over quantum states, the bosonic field  $\phi$  must be periodic under  $\tau \rightarrow \tau + aN_\tau$ .

Similarly, the expectation value of an operator  $O(\phi)$ , which depends on the field  $\phi$ , is given by

$$\langle O \rangle = \int \prod_{\mathbf{x}, \tau} d\phi(\mathbf{x}, \tau) O(\phi) \exp[-S(\phi)] / Z, \quad (9)$$

where we replace the field operator  $\phi$  with its classical value when we insert  $O(\phi)$  in the integrand.

#### D. QCD on the Lattice

For a renormalizable, asymptotically free theory, such as QCD, the lattice formulation takes on a larger significance than just a convenient computational device. The lattice regulates ultraviolet divergences. The lattice constant  $a$  provides an upper bound or “cutoff” scale  $\pi/a$  for momenta. From this point of view the lattice formulation of the theory is every bit as respectable as other regularization schemes. Of course, as usual, we define the theory in the limit in which the cutoff is removed, *i.e.*,  $a \rightarrow 0$ . Before this is done all quantities we calculate have cutoff errors that vanish in the continuum limit.

With the lattice regulator we apply the usual renormalization process: We select a few experimental values and use them to fix the bare parameters of the theory (quark masses and gauge

coupling). In this way the bare parameters depend on the cutoff (lattice spacing), but the physical predictions should approach a cutoff-independent value in the limit of zero lattice spacing. In principle all regularization schemes should agree in the limit that their cutoffs are taken away.

For QCD the fields are fermions and gluons. The groundwork for the lattice formulation of QCD with fermions was laid down by Wilson [7] in 1974, although there was other seminal work on lattice theories with local gauge invariance by Wegner [8], Smit, and Polyakov [9]. To preserve gauge invariance, gluon variables are introduced as  $SU(3)$  matrices on the links between nearest neighbors of the lattice. There are four forward links per site, corresponding to the four components of the color vector potential  $A_\mu^c(x)$ . The matrix for the link joining the site  $x$  with the site  $x + a\hat{\mu}$  is then

$$U_\mu(x) = \exp[igaA_\mu^c(x)\lambda^c/2], \quad (10)$$

where  $\lambda^c$  are the Gell-Mann generators of  $SU(3)$ .

For the pure Yang-Mills theory of gluons a simple lattice form of the classical action is constructed from the plaquettes  $U_{P,\mu\nu}(x)$ , *i.e.*, the product of the link matrices surrounding the unit square in the forward  $\mu\nu$  direction at site  $x$ . The single-plaquette Wilson action is simply the sum over all such plaquettes:

$$S_G(U) = \sum_{x,\mu,\nu} \frac{\beta}{6} \text{ReTr}[1 - U_{P,\mu\nu}(x)], \quad (11)$$

The gauge coupling  $\alpha_s = g^2/4\pi$  appears in the coefficient

$$\beta = 6/g^2. \quad (12)$$

In the continuum limit the plaquette reduces to the familiar square of the field strength tensor summed over eight colors  $c$ :

$$\text{ReTr}[1 - U_{P,\mu\nu}(x)] \rightarrow \frac{g^2 a^4}{4} \sum_c (F_{\mu\nu}^c)^2 + O(a^6). \quad (13)$$

In fact any closed planar loop, normalized by the area in lattice units, has the same continuum limit, but with a different  $O(a^6)$  cutoff error. For example a  $2 \times 1$  rectangular version of the plaquette could also be used. If the two components are combined with the proper choice of coefficients, one can construct an improved gluon action that eliminates the leading cutoff correction, leaving errors at the next order  $O(a^8)$ . Relative to the leading continuum contribution, which carries the volume factor  $a^4$ , such actions are called “tree-level  $O(a^2)$ ” improved. Further improvements can even eliminate quantum cutoff corrections of the type  $O(a^2\alpha_s)$ . The “tadpole Lüscher-Weisz”

actions [10, 11] are in this category. Improving actions in this way is desirable, since it brings a calculation closer to the continuum limit at a given lattice spacing [12].

The quark fields  $\psi(x)$ , one for each flavor, have values on each lattice site. Since they are fermions, they require special treatment in the functional integration: their classical values are anticommuting Grassmann numbers. The fermion contribution to the action for each flavor can be written generally as

$$S_F(U, \psi) = \sum_{x,y} \bar{\psi}(x) M(U, x, y) \psi(y), \quad (14)$$

where  $M(U, x, y)$  is the Dirac matrix – essentially a lattice rendering of the familiar Dirac operator  $\not{D} + m$ . The functional integral for the partition function then becomes

$$Z = \int [dU][d\psi][d\bar{\psi}] \exp[-S_G(U) - S_F(U, \psi)]. \quad (15)$$

Since the dependence on the quark fields is simply bilinear, and computing numerically with anticommuting numbers is nontrivial, it is standard to integrate out the quark fields immediately, following the rules of Grassmann integration, leaving only an integration over the gauge fields, weighted by the determinant of the Dirac matrix:

$$Z = \int [dU] \exp[-S_G(U)] \det[M(U)]. \quad (16)$$

There are many ways to formulate a lattice fermion action, each with its advantages and disadvantages. A great deal of effort over the past couple of decades has been devoted to improving the lattice treatment of fermions. We sketch the formulations here. For more detail, see [4, 5, 6].

### 1. Wilson fermions

The original Wilson rendering of the Dirac operator  $D_V \gamma_V + m$  starts from a simple central difference approximation to the derivative:

$$\nabla_V \psi(x) = \frac{1}{2a} [U_V(x) \psi(x + \hat{v}a) - U_V^\dagger(x - \hat{v}a) \psi(x - \hat{v}a)], \quad (17)$$

where the link matrices  $U_V(x)$  provide the gauge-covariance. The action constructed from this operator is

$$S_{F,\text{naive}} = \sum_{x,v} \bar{\psi}(x) (\nabla_V \gamma_V + m) \psi(x). \quad (18)$$

It describes sixteen degenerate particles where only one is desired. Wilson remedied this undesirable “fermion doubling” problem by adding an irrelevant term to the action

$$S_{F,\text{Wilson}} = S_{F,\text{naive}} - \frac{ar}{2} \sum_{x,\nu} \bar{\psi}(x) \Delta_\nu \psi(x), \quad (19)$$

where  $r$  is usually set to 1 and  $\Delta_\nu \psi(x)$  is the covariant Laplacian,

$$\Delta_\nu \psi(x) = \frac{1}{a^2} [U_\nu(x) \psi(x + \hat{\nu}a) + U_\nu^\dagger(x - \hat{\nu}a) \psi(x - \hat{\nu}a) - 2\psi(x)]. \quad (20)$$

The added term gives fifteen of the doublers masses of order of the cutoff scale  $1/a$ , leaving only one light state. The unwanted doublers thus become inaccessibly heavy in the continuum limit.

It is customary to rearrange the terms in the Wilson action and multiply the field  $\psi(x)$  by a constant to give

$$S_{F,\text{Wilson}} = \bar{\psi}(x) \psi(x) + \kappa \sum_{x,\nu} \bar{\psi}(x) \left[ (1 + \gamma_\nu) U_\nu(x) \psi(x + \hat{\nu}a) + (1 - \gamma_\nu) U_\nu^\dagger(x - \hat{\nu}a) \psi(x - \hat{\nu}a) \right], \quad (21)$$

where the “hopping parameter”  $\kappa = 1/(8 + 2ma)$  controls the quark mass. Improvements to the Wilson formalism include removing tree-level  $O(a)$  errors by introducing a “clover” term in the action [13] and, for two flavors, introducing a “twisted mass” [14, 15].

For thermodynamics applications the chief drawback of Wilson fermions has been (1) an explicit breaking of chiral symmetry at nonzero lattice spacing, (2) a difficulty reaching low quark masses, and (3) a relatively poor representation of the quark dispersion relation. None of these difficulties is insurmountable. Chiral symmetry is restored in the continuum limit.

It is necessary to search for the value  $\kappa = \kappa_c$  where the pion mass vanishes. Since this value depends on the inverse gauge coupling  $\beta$ , one gets a curve  $\kappa_c(\beta)$  in bare parameter  $\kappa - \beta$  space as shown in Fig. 1. Lines of constant pion mass form a family of such curves (not shown) with the pion mass increasing as  $\kappa$  decreases. Also shown is a high temperature crossover line  $\kappa_f(\beta)$ . Its location depends on  $N_\tau$ . Where it intersects the  $\kappa_c$  line, we expect a true chiral phase transition. Pushing to stronger coupling (smaller  $\beta$ ) or negative quark masses (higher  $\kappa$ ) from there takes us into the realm of lattice artifacts: the theory has a parity broken phase at unphysical values of the bare parameters, as indicated.



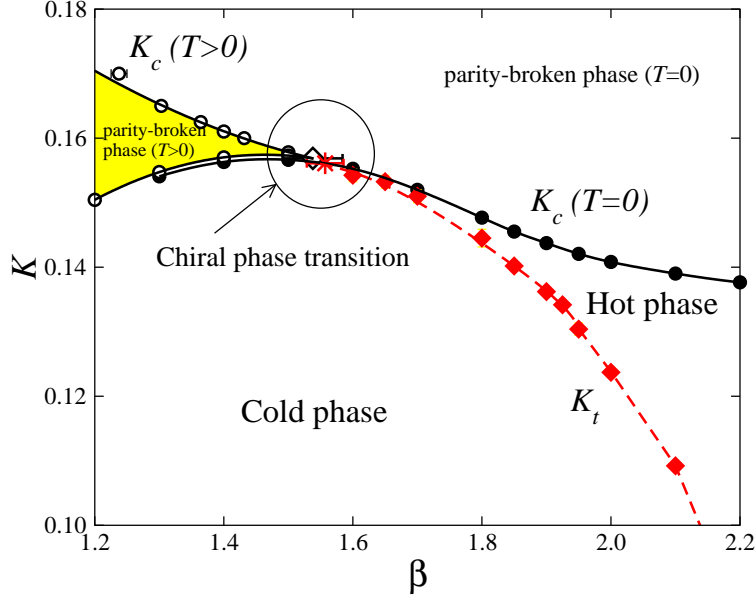


FIG. 1: The bare-parameter phase diagram for two flavors of clover-improved Wilson fermions and an improved gauge action for zero and nonzero temperatures, illustrating the mapping necessary for thermodynamics studies with Wilson fermions. In this plot the hopping parameter  $\kappa$  is denoted by  $K$ . The line of chiral critical hopping parameters  $\kappa_c(T=0)$  was determined from the vanishing of the pion mass. The line  $\kappa_t$  indicates the high temperature crossover at  $N_\tau = 4$ . It was determined from the Polyakov line (see section III A). The region “chiral phase transition” shows where the thermal crossover happens for small pion masses. The parity broken phases come from lattice artifacts of Wilson fermions. The data are from the CP-PACS collaboration, [16], as shown in [17].

## 2. Staggered fermions

The staggered fermion approach starts from the naive action in Eq. (18). Through a field transformation, the Dirac matrices can be diagonalized exactly giving four identical actions, each of them with one spin per site. If we keep only one of the actions, we reduce the lattice fermion degrees of freedom by a factor of four, which still leaves us with four fermion doublers. These residual degrees of freedom are called “tastes.” Without further intervention, they would overcount the sea quark effects by a factor of four. To get approximately the correct counting, we replace the fermion determinant by its fourth root for each of the desired flavors:

$$Z_{\text{stagg}} = \int [dU] \exp[-S_G(U)] \prod_i \det[M_i(U)]^{1/4}. \quad (22)$$

In the continuum limit at nonzero quark masses, the eigenvalues of the determinant cluster in increasingly tighter quartets as expected from fermion doubling [18]. Then we have an  $SU(4)$  taste symmetry, so taking the fourth root is equivalent to using only one of them as a sea quark species. This procedure has generated considerable controversy. Although there is no rigorous proof that the method is valid, all indications so far are that the approximation is under control as long as we take the continuum limit before we take the quark masses to zero or fit data to a chiral model with taste symmetry breaking properly included [19], in which case the limits are completely under control.

At nonzero lattice spacing the taste symmetry is broken, which introduces lattice artifacts. For example, mesons composed of a valence quark and antiquark come in nondegenerate taste multiplets of sixteen tastes. In the continuum limit they are degenerate.

The asqtad [20, 21, 22, 23, 24, 25, 26, 27, 28] and p4fat3 [29, 30] improvements of the staggered fermion formalism eliminate errors of  $O(a^2)$  in the quark dispersion relation and suppress taste splitting significantly. The asqtad suppression is somewhat better, presumably because it eliminates all tree level  $O(a^2)$  errors. The recently proposed HISQ action does still better [31]. In Fig. 2 we compare the predicted and measured scaling of the splitting in the asqtad pion taste multiplet.

Taste splitting can also be reduced simply by replacing the gauge link matrices in the action by smoothed gauge links – for example the Dublin “stout links” [32]. Unlike the asqtad approach, this method does not eliminate  $O(a^2)$  errors systematically. Thus the free quark dispersion relation is still unimproved.

Is taste-symmetry breaking really a problem for thermodynamics? It is believed to be most dramatic for the pion and less noticeable for more massive states [33]. One could argue that close to the crossover temperature and away from the critical point, so many excited states participate, as in the hadron resonance gas model, that pions do not matter much. But if we approach the critical point at fixed lattice spacing, taste splitting is likely to have a strong effect on the critical behavior: we may even get a chiral symmetry restoring transition in the wrong universality class. And certainly at quite low temperatures where pions dominate the statistical ensemble, taste splitting makes a difference.

Taste-symmetry breaking also complicates the definition of the “physical” quark mass in a thermodynamics simulation. At zero temperature it is traditional to adjust the up and down quark masses so that the Goldstone pion (the lightest one in the taste multiplet) has the physical pion

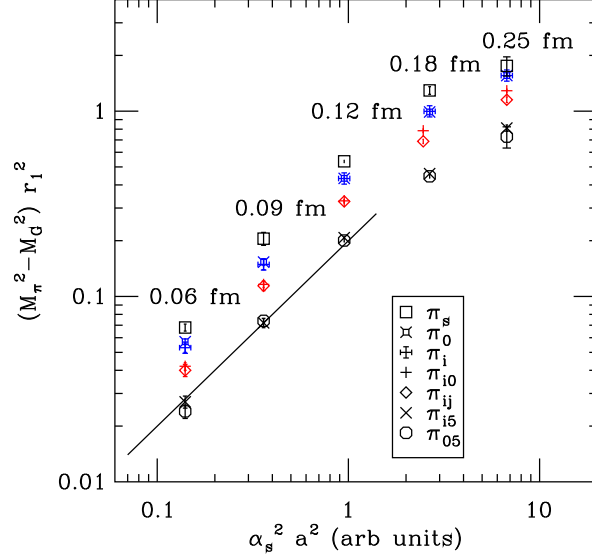


FIG. 2: Plot showing that the lattice artifact taste splitting of pion masses vanishes as  $\alpha_s^2 a^2$  in the continuum limit. The splitting is measured as the difference of the squared masses of the multiplet member and the Goldstone pion member. It is given in units of  $r_1 \approx 0.318$  fm. The plot symbols distinguish the members of the multiplet. (The subscripts in the legend denote the Dirac-gamma-matrix-style classification of the pion tastes, ranging from singlet ( $s$ ) and  $\gamma_0$  to  $\gamma_0\gamma_5$ .) The line is drawn with unit log-log slope to test proportionality to  $\alpha_s^2 a^2$ .

mass. This is legitimate, because we may restrict our attention to Green's functions whose external legs are the Goldstone pion. In a thermodynamics simulation, however, all members of the taste multiplet participate in the thermal ensemble. Thus it is more appropriate to tune the average multiplet mass, *e.g.*, the rms pion mass to the physical pion mass. At a nonzero lattice spacing, the multiplet splitting may be so large, that goal is unreachable. In that case the physical point is reached only by reducing the lattice spacing together with the light quark mass. It is simply incorrect to claim a thermodynamics calculation is done at a physical pion mass when the rms mass is still much higher.

### 3. Domain-wall fermions

Neither the Wilson fermion formulation, including the clover-improved and twisted-mass version, nor the staggered fermion formulation are entirely satisfactory discretizations of fermions. Wilson fermions explicitly break chiral symmetry and its recovery requires a fine tuning. Stag-

gered fermions, while preserving a remnant of chiral symmetry, have a remaining doubling problem, requiring the fourth-root trick, which is still somewhat controversial.

A more sophisticated, somewhat indirect and more costly discretization of fermions goes under the name of “domain-wall fermions” and was developed by Kaplan [34] and by Furman and Shamir [35]. Furman and Shamir’s construction has become standard. An additional, fifth dimension of length  $L_s$  is introduced and one considers 5-d Wilson fermions with no gauge links in the fifth direction, and the 4-d gauge links independent of the fifth coordinate,  $s$ ,

$$S_{DW} = \sum_{s=0}^{L_s-1} \sum_x \bar{\Psi}(x, s) \left\{ \sum_{\mu} \left( \gamma_{\mu} \nabla_{\mu} - \frac{1}{2} \Delta_{\mu} \right) \Psi(x, s) - M \Psi(x, s) - P_- \Psi(x, s+1) - P_+ \Psi(x, s-1) \right\}, \quad (23)$$

where  $P_{\pm} = \frac{1}{2}(1 \pm \gamma_5)$  are chiral projectors and we have set  $r = a = 1$ . The parameter  $M$ , often referred to as domain-wall height, is introduced here with a sign opposite that of the usual mass term for Wilson fermions [Eq. (19)]. It needs to be chosen in the interval  $0 < M < 2$ . For free fermions the optimal choice is  $M = 1$ , while in the interacting case  $M$  should be somewhat larger. The fermion fields satisfy the boundary condition in the fifth direction,

$$P_- \Psi(x, L_s) = -m_f P_- \Psi(x, 0), \quad P_+ \Psi(x, -1) = -m_f P_+ \Psi(x, L_s - 1), \quad (24)$$

where  $m_f$  is a bare quark mass.

The domain-wall fermion action, Eq. (23), has 5-d chiral zero modes  $\Psi$  bound exponentially to the boundaries at  $s = 0$  and  $s = L_s - 1$ , which are identified with the chiral modes of 4-d fermions as,

$$q^R(x) = P_+ \Psi(x, L_s - 1), \quad q^L(x) = P_- \Psi(x, 0), \quad \bar{q}^R(x) = \bar{\Psi}(x, L_s - 1) P_-, \quad \bar{q}^L(x) = \bar{\Psi}(x, 0) P_+. \quad (25)$$

The left- and right-handed modes  $q^L$  and  $q^R$  do not interact for  $m_f = 0$  when  $L_s \rightarrow \infty$  and the domain-wall action has a chiral symmetry. At finite  $L_s$  the chiral symmetry is slightly broken. A popular measure of the chiral symmetry breaking is called “residual mass”,  $m_{res}$ . It is determined from the axial Ward identity applied at the midpoint between the two domain walls, as sketched in Fig. 3. This residual mass was expected to fall off exponentially in  $L_s$ . But, due to lattice artifacts of Wilson fermions with large negative mass, there is a contribution to  $m_{res}$  that decreases only like  $1/L_s$  [36, 37]. An example from a recent dynamical domain-wall fermion simulation [38] is shown in Fig. 4. Nevertheless, often  $L_s = O(10 - 20)$  is large enough to keep the chiral symmetry breaking negligibly small, especially at smaller lattice spacing (weaker coupling).

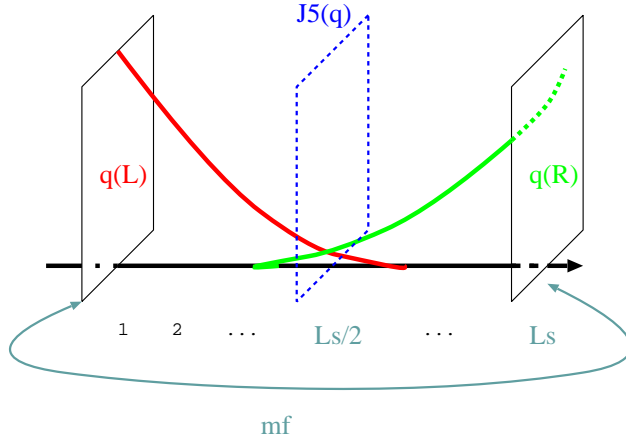


FIG. 3: Sketch, courtesy of Taku Izubuchi, of the domain-wall fermion setup. Left and right handed modes are exponentially bound to the left and right domain walls. The residual mass  $m_{res}$  is determined from an axial Ward identity applied in the center slice.

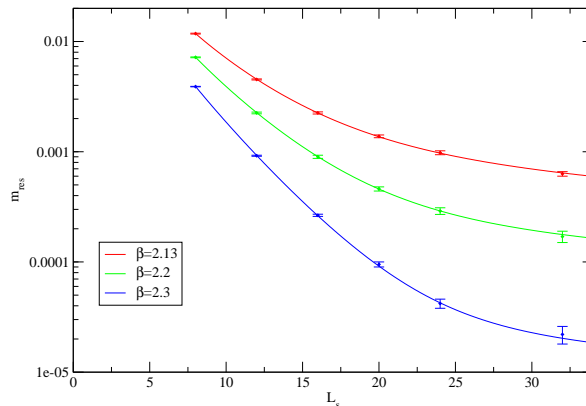


FIG. 4: Plot of the residual mass  $m_{res}$  as a function of  $L_s$  showing its desired suppression with increasing  $L_s$  and increasing inverse gauge coupling  $\beta$ . Also shown are fits to an exponential fall-off plus a  $1/L_s$  contribution, from a recent  $2+1$  flavor dynamical domain-wall fermion simulation [38].

Domain-wall fermions, therefore, solve, or at least substantially alleviate, explicit chiral symmetry breaking without a doubling problem. The price is a computational cost roughly a factor of  $L_s$  larger than that for Wilson type fermions.

Early,  $N_\tau = 4$  nonzero-temperature domain-wall fermion simulations suffered from large residual mass, since the lattice spacing in the transition/crossover region is large, leading to much heavier quarks than desired [39]. More recent simulations with  $N_\tau = 8$ , still using  $L_s = 32$  and

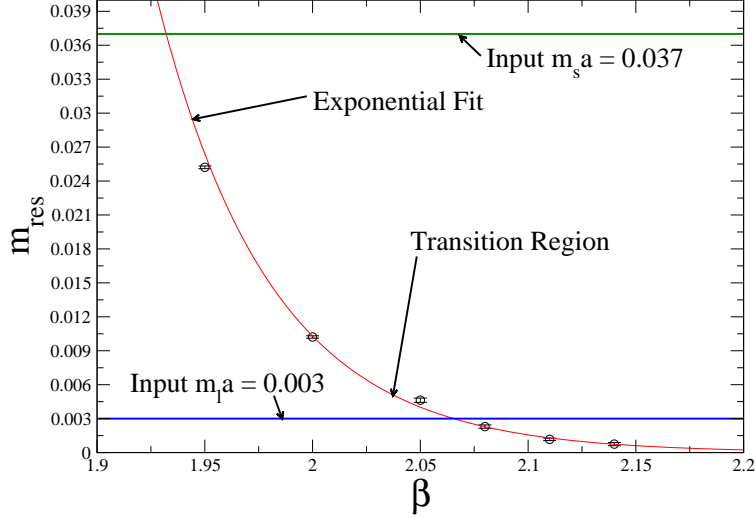


FIG. 5: Residual mass  $m_{res}$  for the recent nonzero-temperature simulations on  $N_t = 8$  lattices with  $L_s = 32$  [40]. At lower  $\beta$ , corresponding to lower temperatures,  $m_{res}$  increases rapidly, and is larger than the input light quark mass already in the transition region.

even 96 are described in [40]. Even for the  $L_s = 32$  simulations with  $N_t = 8$  the residual mass is uncomfortably large in the transition region, and getting worse at lower temperatures, corresponding to smaller  $\beta$  as shown in Fig. 5, since one would like  $m_{res}$  to be small compared with the input light quark masses.

#### 4. Overlap fermions

Related to the domain-wall fermions of the previous subsection are the so-called overlap fermions developed by Narayanan and Neuberger [41, 42]. They retain a complete chiral symmetry without the doubling problem, albeit again at substantial additional computational cost.

The overlap Dirac operator for massless fermions can be written as [42],

$$aD_{ov} = M [1 + \gamma_5 \varepsilon(\gamma_5 D_W(-M))] , \quad (26)$$

where  $D_W(-M)$  is the usual Wilson Dirac operator with negative mass  $m = -M$ . As with domain-wall fermions  $0 < M < 2$  should be used. For a hermitian matrix  $X$ ,  $\varepsilon(X)$  is the matrix sign function, that can be defined as

$$\varepsilon(X) = \frac{X}{\sqrt{X^2}} . \quad (27)$$

Using the fact that  $\varepsilon^2(X) = 1$  it is easy to see that the Neuberger-Dirac operator satisfies the so-called Ginsparg-Wilson relation [43],

$$\{\gamma_5, D_{ov}\} = aD_{ov}\gamma_5RD_{ov}, \quad (28)$$

with  $R = 1/M$ . Equivalently, when the inverse of  $D_{ov}$  is well defined, it satisfies

$$\{\gamma_5, D_{ov}^{-1}\} = a\gamma_5R. \quad (29)$$

Chiral symmetry, in the continuum, implies that the massless fermion propagator anticommutes with  $\gamma_5$ . As seen above, the massless overlap propagator violates this only by a local term that vanishes in the continuum limit. According to Ginsparg and Wilson this is the mildest violation of the continuum chiral symmetry on the lattice possible. Lüscher [44] has shown that any Dirac operator satisfying the Ginsparg-Wilson relation (28) has a modified chiral symmetry at finite lattice spacing,

$$\delta\psi = i\varepsilon\gamma_5\left(1 - \frac{a}{2M}D\right)\psi, \quad \delta\bar{\psi} = i\varepsilon\bar{\psi}\left(1 - \frac{a}{2M}D\right)\gamma_5. \quad (30)$$

or

$$\delta\psi = i\varepsilon\gamma_5\left(1 - \frac{a}{M}D\right)\psi = i\varepsilon\hat{\gamma}_5\psi, \quad \delta\bar{\psi} = i\varepsilon\bar{\psi}\gamma_5, \quad (31)$$

with  $\hat{\gamma}_5 = \gamma_5\left(1 - \frac{a}{M}D\right)$  satisfying  $\hat{\gamma}_5^\dagger = \hat{\gamma}_5$  and, using the G-W relation, Eq. (28),  $\hat{\gamma}_5^2 = 1$ .

So far only one exploratory study, on a  $6^3 \times 4$  lattice, of nonzero-temperature overlap fermions has been done [45]. The main difficulty and computational cost for overlap fermions comes from the numerical implementation of the matrix sign function, Eq. (27).

## E. Cutoff effects

In selecting a fermion formalism for a thermodynamics study, it is important to be aware of possible lattice artifacts (cutoff effects). There are two important categories of artifacts. One comes from an imperfect rendering of chiral symmetry. The other, from the free quark dispersion relation.

It is obviously important to get the chiral symmetry right if we are simulating close to a chiral phase transition. Each action has its problems with chiral symmetry. For staggered fermions the taste splitting interferes. For Wilson fermions, the chiral symmetry is explicitly broken at nonzero lattice spacing. For these actions the obvious remedy is to reduce the lattice spacing. For domain-wall fermions, chiral symmetry is broken to the extent the fifth dimension is not infinite, and,

for overlap fermions, chiral symmetry is broken to the extent the matrix sign function is only approximated in numerical simulations. For the latter two chiral actions, this type of error can be reduced without also reducing the lattice spacing.

At high temperatures where quarks are effectively deconfined, it would seem important to have a good quark dispersion relation, so, for example, we get an accurate value for the energy density and pressure. This artifact can be studied analytically for free fermions. Recently Hegde *et al.* [46] looked at deviations from the expected free-fermion Stefan-Boltzmann relation for the pressure  $p$  as a function of  $1/N_\tau^2$  (equivalently  $a^2$ ) and chemical potential  $\mu/T$ :

$$\frac{p}{T^4} = \sum_{k=0}^{\infty} A_{2k} P_{2k}(\mu/\pi T) \left( \frac{\pi}{N_\tau} \right)^{2k} \quad (32)$$

where  $P_{2k}(\mu/\pi T)$  is a polynomial normalized so that  $P_{2k}(0) = 1$ . The leading term  $A_0$  is the Stefan-Boltzmann term. The ratios of higher coefficients  $A_{2k}/A_0$  measure the strength of the cutoff effects. These terms determine the ability of the action to approximate the continuum free fermion dispersion relation, and they are useful in comparing actions to the extent free quarks are relevant in an interacting plasma. Table I reproduces their results for a variety of actions. We see that the hypercube action [47] has pleasingly small coefficients. The Naik (asqtad) and p4 (p4fat3) actions remove the second order term as designed, but the p4 action is better at sixth order. The standard (unimproved) staggered action (regardless of gauge-link smearing) does as poorly as does the standard (and clover-improved) Wilson actions. The overlap and domain-wall actions constructed from the standard Wilson kernel unfortunately inherit its poor behavior. Improving the kernel fermion action would help to reduce these cutoff effects.

### III. DETERMINING THE TRANSITION TEMPERATURE

We want to know the temperature of the transition from confined hadronic matter to a quark-gluon plasma for two obvious reasons: to interpret experimental data and to understand QCD as a field theory. If the transition is only a crossover, a likely possibility for QCD at the physical value of the quark masses as discussed below, and a true phase transition occurs only at unphysical values of the quark masses, then these two purposes diverge. A crossover temperature is imprecise, so its meaning could vary with the observable, but one can at least speak of a range of temperatures over which phenomenologically interesting changes take place, or one could choose one observable to identify a temperature. A true phase transition has a precise temperature defined by the singularity



action	$A_2/A_0$	$A_4/A_0$	$A_6/A_0$
standard staggered	248/147	635/147	3796/189
Naik	0	-1143/980	-365/77
p4	0	-1143/980	73/2079
standard Wilson	248/147	635/147	13351/8316
hypercube	-0.242381	0.114366	-0.0436614
overlap/ domain wall	248/147	635/147	3796/189

TABLE I: Continuum limit scaling behavior of free massless quarks in various lattice formulations, based on an expansion [Eq. (32)] of the pressure in powers of  $1/N_\tau^2$  from [46]. Shown are ratios of the expansion coefficients to the ideal, leading Stefan-Boltzmann coefficient. A small ratio indicates good scaling.

of the partition function, and all observables capable of producing a signal should agree about the temperature.

In this section we discuss a variety of observables commonly used to detect the transition. In the following sections we discuss what we have learned from them about the phase structure of QCD.

Two observables are traditionally used to determine the temperature of the transition: the Polyakov loop and the chiral condensate. The Polyakov loop is a natural indicator of deconfinement. The chiral condensate is an indicator of chiral symmetry restoration.

### A. Polyakov loop and the free energy of color screening

The Polyakov loop is an order parameter for a high-temperature, deconfining phase transition in QCD in the limit of infinite quark masses. At finite quark masses it is no longer an order parameter, but it is still used to locate the transition. It is built from the product of time-like gauge-link matrices. It is the expectation value of the color trace of that product:

$$L(\mathbf{x}, a, T) = \left\langle \text{Tr} \prod_{\tau=0}^{N_\tau-1} U_0(\mathbf{x}, \tau) \right\rangle. \quad (33)$$

This quantity is gauge invariant because the combined boundary conditions for gluon and fermion fields require that gauge transformations be periodic under  $t \rightarrow t + N_\tau$ . Translational invariance insures that it is independent of  $\mathbf{x}$ . It can be shown that the Polyakov loop measures the change in the free energy of the ensemble under the introduction of a static quark (excluding its mass).

$$L(a, T) = \exp[-F_L(a, T)/T]. \quad (34)$$

In that sense the Polyakov loop is a useful phenomenological quantity as we now explain. When a static quark is introduced it must be screened so that the ensemble remains a color singlet. At low temperatures, screening is achieved by binding to it the lightest antiquark, forming a static-light meson. The free energy cost then consists of the self-energy of the static charge, the binding energy, and the self-energy of the light quark. In the quark plasma, color neutrality is achieved through a collective shift of the plasma charges, as in Debye screening in an ordinary electrical plasma. Aside from the self-energy of the static quark, which is the same at all temperatures, the additional free energy cost is small. So we expect  $F_q(a, T)$  to decrease abruptly in the transition from the confining regime to the plasma regime.

The static-quark self energy diverges as  $1/a$  in the limit of small lattice spacing, so it is convenient to remove it from the definitions of the free energy and the Polyakov loop:

$$F_L(a, T) = F_{\text{static}}(a) + F_q(T) \quad L_{\text{renorm}}(T) = \exp[-F_q(T)/T]. \quad (35)$$

Figure 6 illustrates the free energy from a recent lattice simulation. (Here and elsewhere, the temperature scale is given in MeV and in units of the Sommer parameter [48],  $r_0 \approx 0.467$  fm. The latter is defined in terms of the potential  $V(r)$  between a heavy quark and antiquark. It is the distance where  $r^2 dV(r)/dr = 1.65$ .) The renormalized free energy behaves as expected.

If we take the masses of all the quarks to infinity, we arrive at the pure  $SU(3)$  Yang-Mills ensemble, which has a first-order deconfining phase transition with zero  $L(a, T)$  at low temperatures and nonzero at high temperatures. The free energy is correspondingly infinite for  $T < T_c$  and finite above. In this limit the Polyakov loop is a true order parameter for the transition.

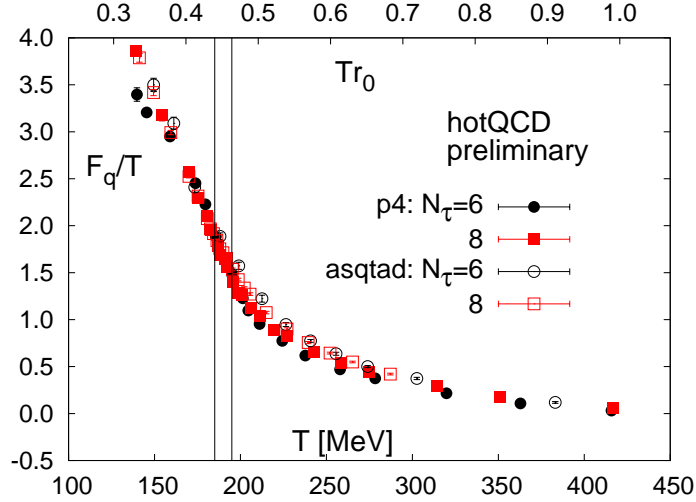


FIG. 6: Renormalized screening free energy of a static quark (from the renormalized Polyakov loop) vs. temperature in MeV units (bottom scale) and  $r_0$  units (top scale) for  $N_\tau = 6$  and 8 from a HotQCD study comparing p4fat3 and asqtad staggered fermion formulations [49, 50, 51]. Measurements are taken along a line of constant physics with  $m_{ud} = 0.1m_s$ . The vertical bands here and in HotQCD figures below indicate a temperature range 185 - 195 MeV and serve to facilitate comparison.

## B. Chiral condensate

### 1. Chiral symmetry restoration

The second traditional observable is the chiral condensate. It is the order parameter for a high-temperature, chiral-symmetry restoring phase transition at zero up and down quark masses. At nonzero quark masses, it is no longer an order parameter, but, like the Polyakov loop, it is used as an indicator of the transition. It is defined for each quark flavor  $i$  as the derivative of the thermodynamic potential  $\ln Z$  with respect to the quark mass,

$$\langle \bar{\Psi}_i(x)\Psi_i(x) \rangle = \frac{T}{V} \frac{\partial \ln Z}{\partial m_i} = \frac{T}{V} \langle \text{Tr} M_i^{-1} \rangle, \quad (36)$$

or the expectation value of the trace of the inverse of the fermion matrix. When the  $u$  and  $d$  quark masses both vanish, QCD has a  $U(1) \times SU(2) \times SU(2)$  chiral symmetry, which is spontaneously broken at low temperatures to  $U(1) \times SU(2)$ , *i.e.*, the familiar baryon number and isospin symmetries. At high temperatures the full chiral symmetry is restored. The chiral condensate  $\langle \bar{\Psi}\Psi \rangle$  is the order parameter of the broken symmetry. It is nonzero at low temperatures and zero at high

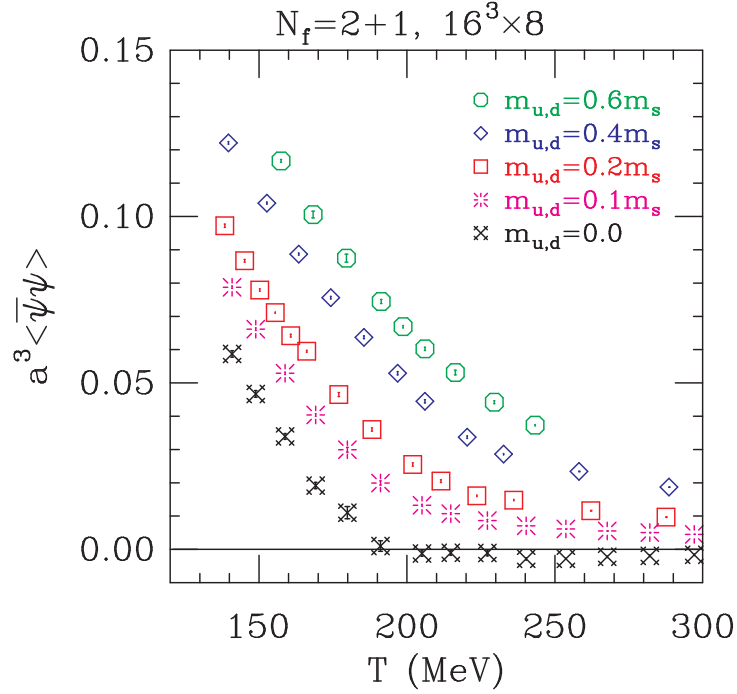


FIG. 7: Chiral condensate vs. temperature in MeV units ( $r_0$  scale) for  $N_\tau = 8$  from [52] using the asqtad fermion formulation. Measurements were taken along lines of constant physics with a range of light, degenerate up and down quark masses  $m_{ud}$  specified in the legend as a fraction of the strange quark mass  $m_s$ . An extrapolation to zero quark mass is also shown.

temperatures. With only two flavors, the phase transition is expected to be second order, so the chiral condensate is continuous at the transition. When the quark masses are small, but nonzero, as they are in nature, the symmetry is explicitly broken and the chiral condensate does not vanish at high temperatures, but it is small.

Figure 7 illustrates the behavior of the chiral condensate from a recent lattice simulation with two light quark flavors and one massive strange quark. Measurements were taken along “lines of constant physics”, *i.e.*, curves in the space of the bare parameters (gauge coupling and quark masses) along which the pion and kaon masses are approximately constant, whether or not they have their correct experimental values. The extrapolation to zero light quark mass appears to be consistent with the expected behavior of this chiral order parameter.

## 2. *Chiral multiplets*

The restoration of chiral symmetry leads to symmetry multiplets in the hadronic spectrum. At low temperatures, where the symmetry is spontaneously broken, the spectrum consists of the familiar hadrons. At high temperatures, where the symmetry is restored, they may have analogs as resonant plasma excitations, at least not too far above the crossover temperature. They also control screening in the plasma in analogy with the Yukawa interaction. (See Sec. VII B.)

When the light quarks are massless, spontaneous symmetry breaking requires that the pion be massless. If the symmetry is restored at high temperatures, the pion, suitably defined as a state, acquires a mass. Of course, in nature, the light quarks are not massless, so the symmetry is only approximate, and the pion has a small mass at low temperatures.

Another consequence of restoring the chiral symmetry with massless  $u$  and  $d$  quarks is that all hadronic states involving those quarks would fall into larger symmetry multiplets. Thus, for example, the three pions become degenerate with the  $f_0$ , the three  $a_0$ 's become degenerate with the  $\eta$ , and nucleons become degenerate with parity-partner nucleons.

The classical QCD Lagrangian suggests a further  $U(1)$  chiral symmetry, which would conserve a flavor-singlet axial charge. This symmetry is broken at the quantum level. This quantum phenomenon is called the Adler-Bell-Jackiw axial anomaly [53]. Whether the strength of the anomaly decreases in conjunction with the high temperature transition is an open question.

If the anomaly also vanishes, the eight meson states listed above fall into a single degenerate supermultiplet. Again, if the light quarks are not precisely massless or the anomaly does not completely vanish, these statements are only approximate.

Whether or not hadron-like resonances are observable in experiments, the multiplets appear, nonetheless, in calculations, most notably in simulations of hadronic screening.

## 3. *Singularities of the chiral condensate*

Although we require a numerical simulation to determine the chiral condensate, from general considerations we can predict some of its singularities at small quark mass  $m$  and small lattice

spacing  $a$ :

$$\langle \bar{\psi}\psi(a, m, T) \rangle \sim \begin{cases} c_{1/2}(a, T)\sqrt{m} + c_1 m/a^2 + \text{analytic} & T < T_c, \\ c_1 m/a^2 + c_\delta m^{1/\delta} + \text{analytic} & T = T_c, \\ c_1 m/a^2 + \text{analytic} & T > T_c. \end{cases} \quad (37)$$

Knowing the behavior of the condensate, and in particular its singularities, is important for locating the phase transition. The  $m/a^2$  singularity is easily derived in perturbation theory from a one-quark-loop diagram. The  $\sqrt{m}$  singularity at low temperatures arises in chiral perturbation theory at one-loop order. In this case the pion makes the loop. It is an infrared singularity caused by the vanishing of the pion mass at zero quark mass [54]. Thus it appears only in the confined phase where the pion is massless. If we take  $T \rightarrow 0$  before  $m \rightarrow 0$  the square root singularity is replaced by the usual chiral  $\log(m)$ . The term  $m^{1/\delta}$  is the expected critical behavior at the transition temperature. [For the expected 3-d  $O(4)$  universality class,  $\delta = 0.56$ .] The RBC-Bielefeld group discusses evidence for the expected mass dependence [54].

In a calculation with three quarks with masses  $m_u = m_d = m_\ell$  and  $m_s$ , it is convenient for comparing results of different calculations to eliminate the ultraviolet divergence by taking a linear combination of the light-quark and strange-quark chiral condensates

$$\begin{aligned} D_{\ell,s}(T) &= \langle \bar{\psi}\psi \rangle|_\ell - \frac{m_\ell}{m_s} \langle \bar{\psi}\psi \rangle|_s, \\ \Delta_{\ell,s}(T) &= D_{\ell,s}(T)/D_{\ell,s}(T=0). \end{aligned} \quad (38)$$

The ratio  $\Delta_{\ell,s}$  of the high-temperature and zero-temperature value also eliminates a common scalar-density renormalization factor  $Z_S$ . This is the quantity plotted in Fig. 8 from a recent simulation. It shows the expected dramatic fall-off at the crossover.

### C. Other Observables

Susceptibilities are often used as indicators of a phase transition. They measure fluctuations in the related observables. Since a transition or crossover is usually accompanied by fluctuations in an order parameter, the related susceptibilities tend to peak there.

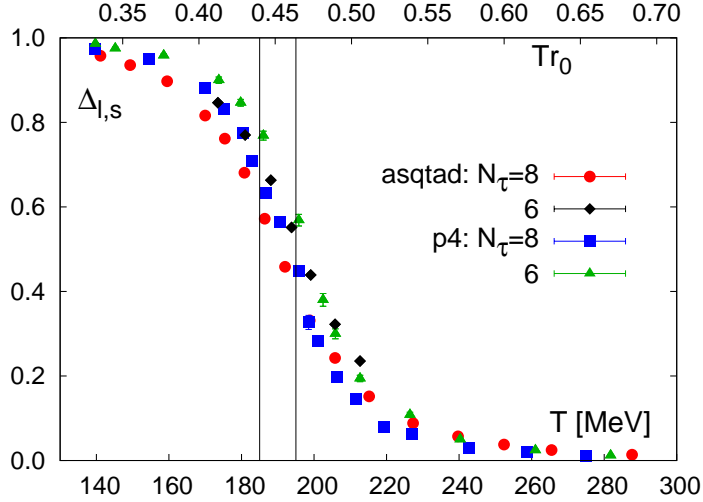


FIG. 8: To give an indication of its variation with lattice spacing, we plot the chiral condensate difference ratio vs. temperature in MeV units (bottom scale) and  $r_0$  units (top scale) for  $N_\tau = 6$  and 8 from a HotQCD study. Results are given for both the p4fat3 and asqtad staggered fermion formulations [51]. Measurements are taken along a line of constant physics with  $m_{ud} = 0.1m_s$ .

### 1. Quark number susceptibility

In the low temperature phase, fluctuations in quark number are suppressed by confinement for the same reason that the free energy of screening of a static quark is large there. At high temperatures, fluctuations are common. There can also be cross-correlations. The relevant observable for a quark of flavor  $i$  is the expectation  $\langle N_i^2/V \rangle$  for spatial volume  $V$  and total quark number  $N_i$ . This is the quark number susceptibility. It controls event-by-event fluctuations in the associated flavor in heavy ion collisions. For flavors  $i$  and  $j$  the generalized susceptibility (including cross correlations) is

$$\chi_{ij} = \langle N_i N_j / V \rangle = \frac{T}{V} \frac{\partial^2 \ln Z}{\partial \mu_i \partial \mu_j}. \quad (39)$$

We discuss the Taylor expansion of this observable in  $\mu_i$  in Sec. VI E.

Figure 9 illustrates the behavior of the strange quark number susceptibility  $\chi_{ss}$ . It shows an abrupt rise at the crossover. Because it has a relatively high signal to noise ratio, this quantity is often used to define the crossover temperature.

We can transform the generalized quark number susceptibility  $\chi_{ij}$  from the flavor basis to the basis in which the isospin  $I$ , hypercharge  $Y$ , and baryon number  $B$  are diagonal. The resulting

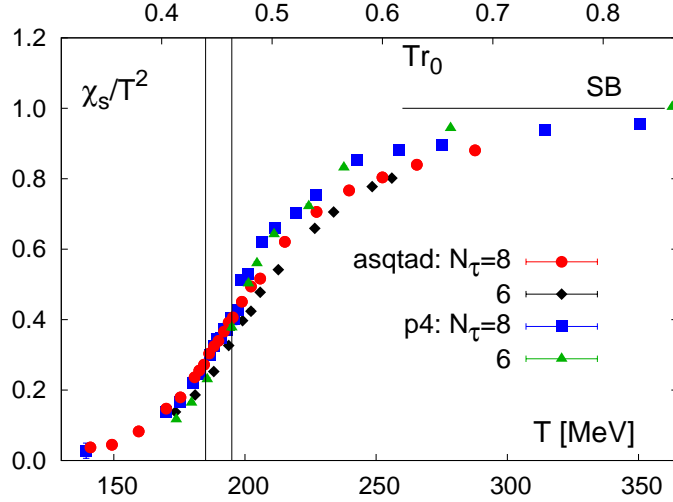


FIG. 9: Strange quark number susceptibility divided by the square of the temperature *vs.* temperature in MeV units (bottom scale) and  $r_0$  units (top scale) for  $N_\tau = 6$  and 8. Measurements are taken along a line of constant physics with  $m_{ud} = 0.1m_s$ . Results are from a HotQCD study comparing p4fat3 and asqtad staggered fermion formulations [51].

quantities are shown in Fig. 10. The diagonal susceptibilities all show the expected abrupt rise at the crossover temperature. The offdiagonal susceptibility  $\chi_{Y,B}$  shows a small nonzero value above the crossover. The positive correlation between hypercharge and baryon number at these temperatures can either be understood in terms of fluctuations in light quark degrees of freedom or in terms of persistent three-quark baryon states: Light up and down quarks have positive baryon number ( $1/3$ ) and hypercharge ( $1/3$ ) and their antiquarks have the opposite values. In both cases their fluctuations lead to a positive correlation. Strange quarks have positive baryon number ( $1/3$ ) but negative hypercharge ( $-2/3$ ). They would lead to a negative correlation, but because of their higher mass, they are less prevalent. So we are left with a net positive correlation. At higher temperatures the mass difference is irrelevant and the correlations cancel. Similar arguments can be made for three-quark baryonic states, where nonstrange baryons are more prevalent than strange baryons.

In Fig. 11 we show a computation of baryon ( $\chi_q$ ) and isospin ( $\chi_I$ ) quark number susceptibilities from a recent computation with two flavors of clover-improved Wilson fermions on  $16^3 \times 4$  lattices [55], using a different normalization from that of Fig. 10. The cutoff effects for this Wilson fermion simulation are seen to be significantly larger than with improved staggered fermions, as expected from Table I.



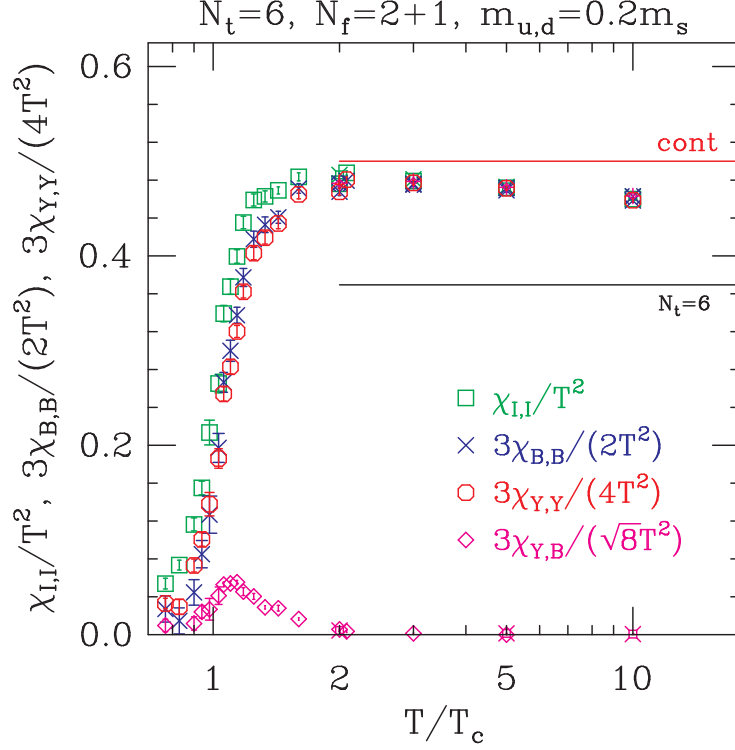


FIG. 10: Chiral susceptibility matrix in the  $I, Y, B$  basis. divided by the square of the temperature vs. temperature in units of the crossover temperature  $T_c$  for  $N_t = 6$ . Measurements are taken along a line of constant physics with  $m_{ud} = 0.2m_s$  from [52].

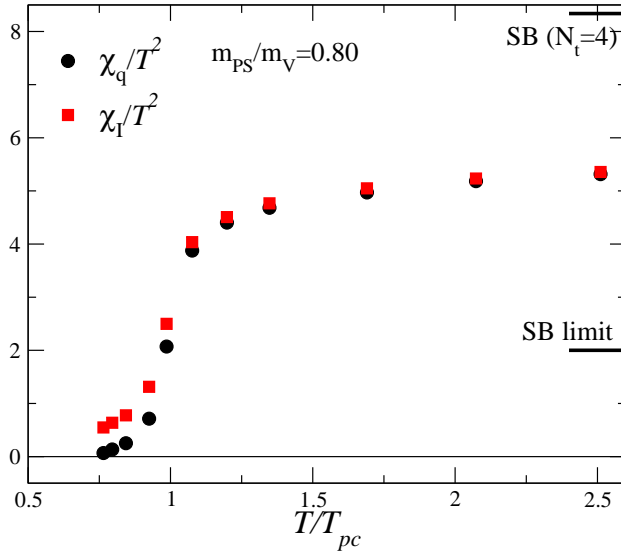


FIG. 11: Quark number susceptibilities with Wilson fermions on  $N_t = 4$  lattices along a line of constant physics with pseudoscalar to vector meson mass ratio  $m_{PS}/m_V = 0.8$  from [55].

## 2. Chiral susceptibility

The various chiral susceptibilities are based on the second derivative of the thermodynamic potential with respect to the quark masses

$$\chi_{ij} = \frac{T}{V} \frac{\partial^2 \ln Z}{\partial m_i \partial m_j}. \quad (40)$$

For two equal mass light quarks  $u$  and  $d$ , the derivatives can be converted to expectation values of products of the inverse of the fermion Dirac matrix  $M$  for those species. The commonly reported susceptibilities are the “disconnected” chiral susceptibility

$$\chi_{\text{disc}} = \frac{T}{V} \left[ \langle (\text{Tr} M^{-1})^2 \rangle - \langle \text{Tr} M^{-1} \rangle^2 \right], \quad (41)$$

the connected chiral susceptibility

$$\chi_{\text{conn}} = \frac{T}{V} \langle \text{Tr} M^{-2} \rangle, \quad (42)$$

the isosinglet susceptibility

$$\chi_{\text{sing}} = \chi_{\text{conn}} + 2\chi_{\text{disc}}, \quad (43)$$

and the isotriplet susceptibility

$$\chi_{\text{trip}} = 2\chi_{\text{conn}}. \quad (44)$$

Figure 12 gives an example of the peak in the disconnected chiral susceptibility at the crossover.

Since the chiral susceptibility is the derivative of the chiral condensate with respect to quark mass, one can immediately derive its singularities from the expressions for the condensate in Eq. (37).

$$\chi_{\text{sing}}(a, m, T) \sim \begin{cases} c_{1/2}(a, T)/(2\sqrt{m}) + c_1/a^2 + \text{analytic} & T < T_c, \\ c_1/a^2 + (c_\delta/\delta)m^{1/\delta-1} + \text{analytic} & T = T_c, \\ c_1/a^2 + \text{analytic} & T > T_c. \end{cases} \quad (45)$$

The RBC-Bielefeld group discusses numerical evidence for the expected mass dependence [54]. Trends in Fig. 12 are consistent with these expectations. In the limit of zero quark mass, this quantity is infinite below the transition and finite above. In the continuum limit it has a temperature-independent ultraviolet divergence. Thus the Budapest/Wuppertal group propose subtracting the zero temperature value, multiplying by the square of the bare quark mass, and dividing by the fourth power of the temperature [32]:

$$m^2 \Delta \chi_{\text{disc}}(a, m, T) / T^4. \quad (46)$$

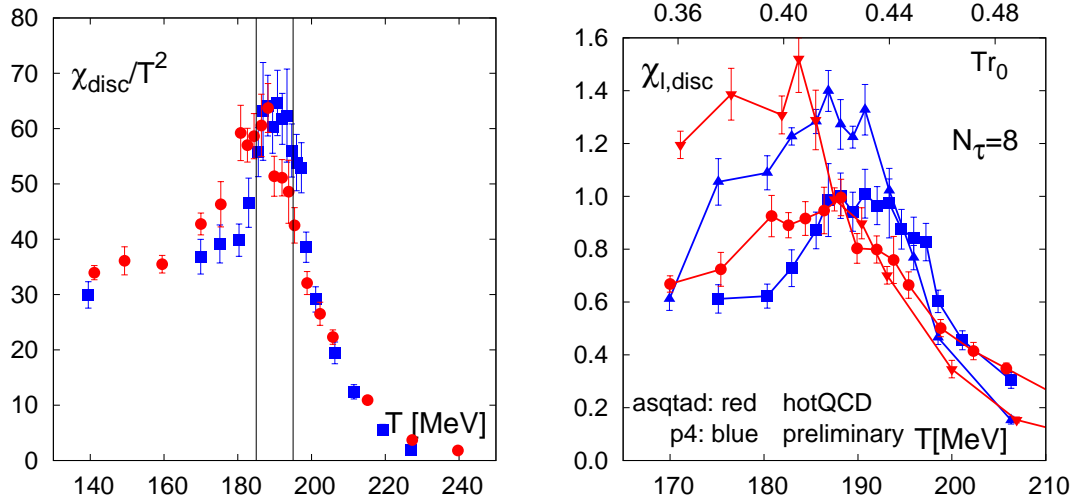


FIG. 12: Left panel: Disconnected light quark susceptibility vs. temperature in MeV ( $r_0$ ) units (bottom scale). Right panel: closeup of the peak region. Lines merely connect the points. Red circles and downward-pointing triangles, asqtad fermions. Blue squares and upward-pointing triangles, p4fat3. Squares and circles are along a line of constant physics with  $m_{ud} = 0.1m_s$ , and triangles, with  $m_{ud} = 0.05m_s$ . All results are HotQCD preliminary [49, 50, 56].

where  $\Delta\chi_{\text{disc}}(a, m, T) = \chi(a, m, T) - \chi(a, m, 0)$ . The  $m^2$  cancels the scalar density renormalization factor. Of course, this quantity vanishes in the zero mass limit.

#### D. Setting the temperature scale

In order to quote dimensionful lattice results in physical units, it is necessary to determine the lattice spacing in physical units. The calibration must be based on a quantity that is reliably determined in zero-temperature lattice simulations. Recent favorites are the splitting of  $\Upsilon$  levels, the mass of the  $\Omega^-$  baryon, and the light meson decay constants, such as  $f_\pi$  or  $f_K$ . These scale determinations are not guaranteed to agree at nonzero lattice spacing and at unphysical values of the quark masses. Indeed, there can be substantial differences. For example, for the asqtad action with a nearly physical strange quark mass, a light quark mass one tenth as heavy, and a lattice spacing of approximately 0.12 fm, the  $f_K$  scale gives a 15% lower temperature than the  $\Upsilon$  splitting scale. For the same quark masses, at approximately 0.09 fm the discrepancy has decreased to 8%, consistent with an approximately  $O(a^2)$  scaling error. Of course, for any quantity of interest, thermodynamic or not, if possible, we would like to choose a scale according to which that quantity

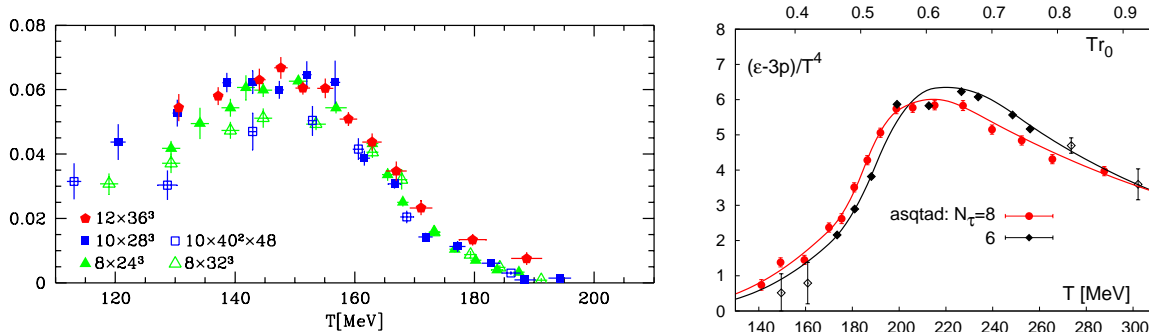


FIG. 13: Left panel: renormalized chiral susceptibility vs temperature ( $f_K$  scale) from [57]. Right panel: interaction measure vs temperature ( $r_0$  scale) from [51]. (See the definition of this quantity in Sec. VIB.) Note that the interaction measure peaks at about 20 MeV above the crossover.

has only a small variation as the lattice spacing approaches zero.

Recent results from Aoki *et al.* [57] give a rather different temperature  $T_c$  for the crossover than the HotQCD collaboration [51]. Aoki *et al.* locate the peak in their renormalized chiral susceptibility at around 150 MeV ( $f_K$ ) for  $N_\tau = 8, 10$ , and 12. The HotQCD collaboration puts the crossover closer to 190 MeV ( $r_0$ ) for  $N_\tau = 8$  and  $m_{ud}/m_s = 0.1$ . Here are possible reasons for the discrepancy:

- Much of the difference comes from the different choice of scale. The Budapest-Wuppertal collaboration uses  $f_K$  to set the scale, and the HotQCD collaboration uses the Sommer parameter  $r_0$ , calibrated ultimately from  $\Upsilon$  splittings [58]. The scale discrepancy alone could explain about 30 MeV of the difference.
- Some of the discrepancy also comes from differences in lattice parameters. The Budapest-Wuppertal collaboration uses a smaller lattice spacing and lighter light quark mass. The HotQCD collaboration estimates an approximately 10 MeV ( $r_0$  scale) downward shift in curves related to the equation of state in the continuum limit with physical quark masses. Some of that shift is visible in the right panel of Fig. 13.
- Some may also come from differences in the fermion formulations. The Budapest-Wuppertal group use standard staggered fermions with stout gauge links. This approach reduces effects of taste splitting, but does not improve the quark dispersion relation as do the actions used by the HotQCD collaboration. We don't know whether such differences would result in a shift in a peak position, however.

Whatever the differences, no matter how one sets the scale, one expects all methods to give the same results for the same observable in the continuum limit at physical quark masses. So for now we are left guessing the result of taking that limit. Since most of the present difference apparently comes from a choice of scale, it would help our guessing to know which scale is more suitable for thermodynamic quantities. We have seen that the chiral susceptibility suffers from peculiar singularities that may make it less suitable for locating the crossover temperature. Still, the left panel of Fig. 13 suggests that it scales reasonably well in  $f_K$  units. For the phenomenology of heavy ion collisions, quantities related more directly to deconfinement, such as the interaction measure (equation of state) and quark number susceptibility are important. As we can see from the right panel of Fig. 13 the interaction measure seems to show better (but still imperfect) scaling in the  $r_0$  scale. (Preliminary HotQCD results for the chiral susceptibility are shown in the  $r_0$  scale in Fig. 12.)

#### IV. QCD PHASE DIAGRAM AT ZERO DENSITY

##### A. General outline of the phase diagram

At infinite quark mass QCD becomes a pure Yang-Mills theory, which has a well-studied, weak, first-order deconfining phase transition [59]. As the quark masses are decreased, the first order transition weakens further and devolves into a crossover, as indicated in Fig. 14, which summarizes in *qualitative* terms the generally accepted phase structure at zero chemical potential in the flavors  $u$ ,  $d$ , and  $s$ .

Close to zero quark mass, chiral perturbation theory applies, and quite general arguments can be made about the qualitative nature of the phase transition [60], depending on the number of quark flavors with zero mass and depending on what happens to the anomaly at the transition. With a nonzero anomaly and only two quark flavors the transition certainly occurs at zero  $u$  and  $d$  quark masses, and it is in the 3-d  $O(4)$  universality class, because of the  $O(4)$  two-flavor chiral symmetry. If the strange quark is also massless, the chiral transition is first order, and, since first order transitions are not usually removed by small symmetry-breaking perturbations, it persists as the quark masses are increased. Eventually, at sufficiently large  $u$ ,  $d$ , and  $s$  quark masses the system is too far from chiral and the first-order transition gives way to a second-order phase transition in the Ising or  $Z(2)$  universality class: Ising, since at nonzero quark masses, there is no remaining

chiral symmetry. In the  $m_u = m_d$  vs  $m_s$  plane a curve of such second order transitions separates the first-order regime from the crossover regime as sketched in the left panel of Fig. 14.

The quantitative determination of the phase boundaries requires numerical simulation. What has emerged is that the second-order critical line occurs at quite small quark masses, where simulations are particularly challenging and especially sensitive to cutoff effects [61, 62]. The right panel of Fig. 14 shows recent results from de Forcrand and Philipsen based on a calculation using unimproved staggered fermions with  $N_\tau = 4$ .

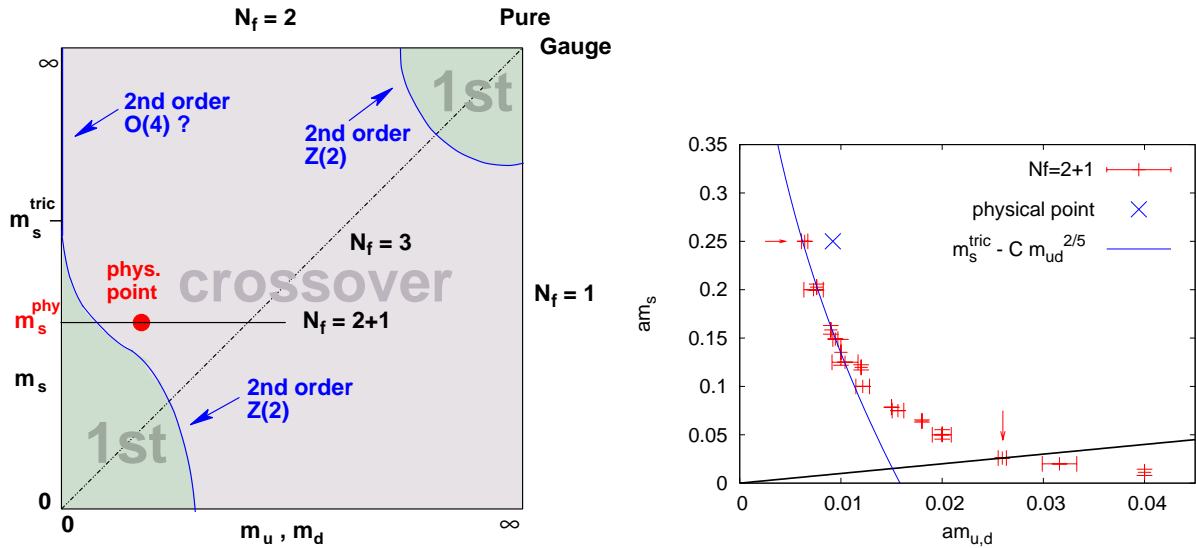


FIG. 14: Left panel: sketch of the phase diagram for QCD at zero baryon density in  $2 + 1$  flavor QCD as a function of the light quark masses showing regions where a high-temperature phase transition or crossover is expected. For a second-order phase transition, the universality class is shown. The physical point is plotted as a dot in the crossover region. Whether the expected tricritical strange quark mass  $m_s^{\text{tric}}$  is higher or lower than the physical strange quark mass  $m_s^{\text{phys}}$  is not yet firmly established. (Similar versions of this figure have appeared in the literature including [63].) Right panel: result of an actual measurement of a portion of the 2nd order  $Z(2)$  phase boundary at  $N_\tau = 4$  from Ref. [64]. The axes give bare quark masses in lattice units and the blue cross marks the physical point.

## B. Order of the phase transition for physical quark masses

A key phenomenological question is whether there is a first order phase transition at the physical value of the  $u$ ,  $d$ , and  $s$  quark masses or there is merely a crossover. All present evidence points to a crossover at zero chemical potential for these species. A recent, thorough investigation has

been carried out by the Budapest-Wuppertal group [65]. They examine the conventional signal of the peak height in the chiral susceptibility, which they renormalize using Eq. (46). If there is no phase transition (*i.e.*, only a crossover), the peak height should be asymptotically constant in the thermodynamic limit of an infinite lattice volume. If there is a first order phase transition, the height is infinite, but it is limited in a finite volume by finite-size effects. Asymptotically, it scales linearly with the lattice volume  $L^3$ . If the transition is second order, the volume dependence is weaker, but the result is still infinite. The Budapest-Wuppertal group ran a simulation with conventional staggered fermions on stout links at  $N_\tau = 4, 6, 8,$  and  $10$ . They analyzed their data in two steps. First they extrapolated the inverse peak height to zero lattice spacing at fixed lattice aspect ratio  $LT$ , as shown in the upper panels of Fig. 15. Then they extrapolated the continuum values to infinite aspect ratio (thermodynamic limit). The result is compared in the lower panel of Fig. 15 with predictions for a first order phase transition and a phase transition in the 3-d  $O(4)$  universality class. The disagreement is a strong indication that there is no phase transition.

### C. Order of the phase transition for two massless flavors

There is a related question of significant theoretical interest. When all quarks but the  $u$  and  $d$  are infinitely massive, we have a two-flavor theory, and, as we have observed above, as long as the chiral anomaly is not involved, we expect a critical point only at zero quark mass. Furthermore, since the two-flavor chiral symmetry  $SU(2) \times SU(2) \simeq O(4)$ , we expect the high-temperature deconfining critical point to be in the 3-d  $O(4)$  universality class.

This question has been investigated by several groups with somewhat contradictory results. Simulations with standard staggered quarks using  $N_\tau = 4$  lattices, with large lattice spacing in the transition region, and hence potentially large lattice artifacts, as collected by T. Mendez [66], show some deviations from  $O(4)$  scaling as shown in Fig. 16. For  $O(4)$  scaling, all data points should collapse to the curve in the figure. Two-flavor clover-improved Wilson fermion simulations [16], on the other hand, indicate good  $O(4)$  scaling as seen in Fig. 17.

Since staggered fermions, at the large lattice spacings in the transition region on high-temperature lattices with small  $N_\tau$ , have quite large taste symmetry breaking, one might expect the transition to be in the  $U(1) \times U(1) \simeq O(2)$  universality class, rather than the  $O(4)$  one. More importantly, Kogut and Sinclair [67] argue that finite volume effects on the fairly small (spatial) lattices used are quite large. Indeed they found good agreement with  $O(2)$  scaling, when taking

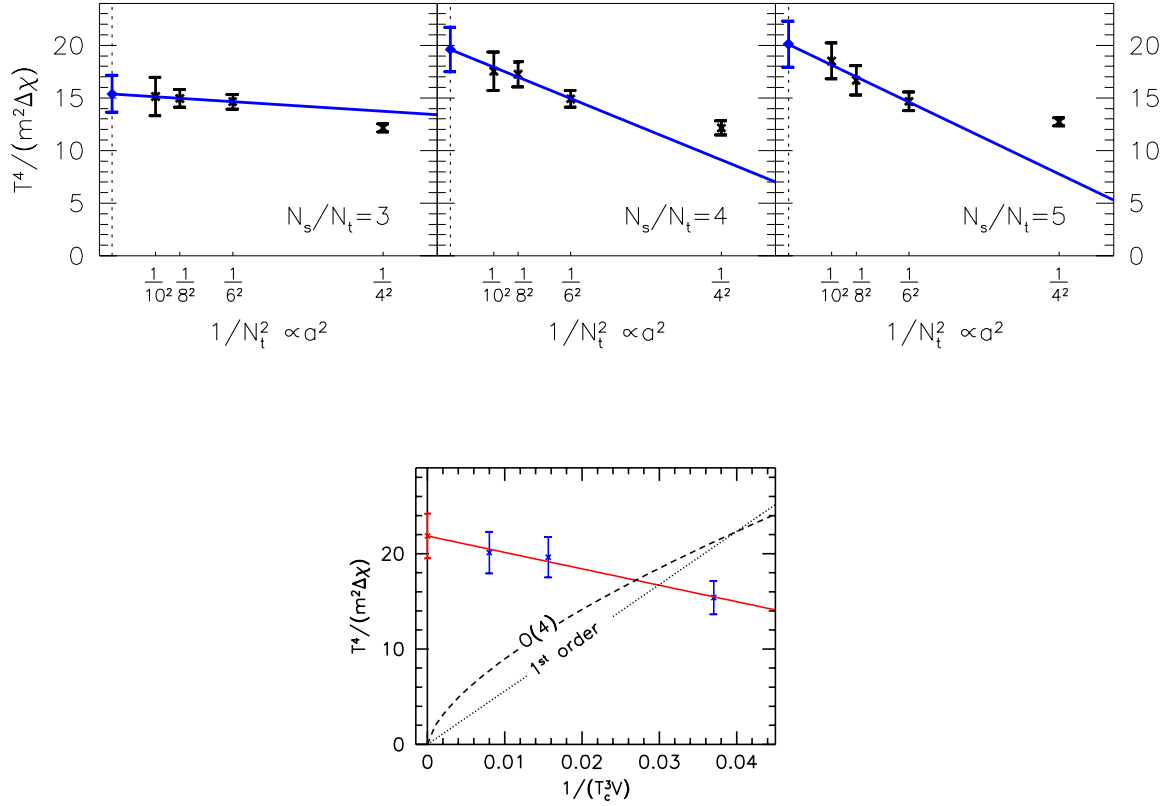


FIG. 15: Results from [65]. Upper panels: Inverse of the peak height in the renormalized disconnected chiral susceptibility vs. squared lattice spacing showing the extrapolation to zero lattice spacing. The lattice aspect ratio is varied from left to right. Lower panel: Inverse of the peak height in the renormalized disconnected chiral susceptibility vs. inverse aspect ratio cubed showing the extrapolation to the thermodynamic limit. Also shown are predictions for a first order phase transition and a second order transition in the 3-d  $O(4)$  universality class.

the finite volume effects into account as illustrated in Fig. 18

In contradiction with the theoretical expectations and the above summarized numerical findings, D’Elia, Di Giacomo, and Pica found indications of a first-order transition using an unimproved staggered fermion action and  $N_\tau = 4$  [68]. It is important to check this conclusion with a more refined action. One should conclude that at present the order of the high-temperature transition with two massless flavors is still an open question.



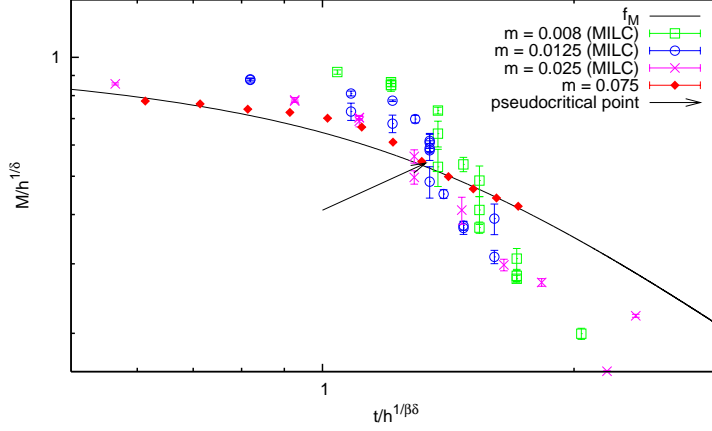


FIG. 16: A double logarithmic plot showing strong deviations from  $O(4)$  scaling in this parameter range for two flavors of staggered fermions using  $N_\tau = 4$  lattices, collected in [66]. The function  $M$  is the chiral condensate (magnetization in the spin system),  $h$  the quark mass (external magnetic field) and  $\beta$  and  $\delta$  are critical exponents.  $t = 6/g^2 - 6/g_c^2$  plays the role of the reduced temperature.

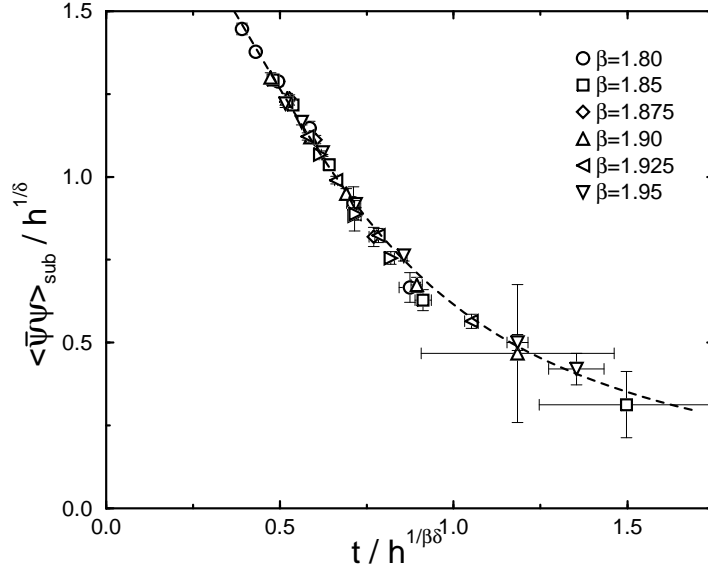


FIG. 17:  $O(4)$  scaling, with linear scale, for two flavors of Wilson fermions using  $N_\tau = 4$  lattices, from [16].

#### D. The phase transition with a physical strange quark

Suppose, instead, we hold the strange quark mass at its physical value and then decrease the  $u$  and  $d$  quark masses toward zero. According to the qualitative picture in the left panel of Fig. 14,

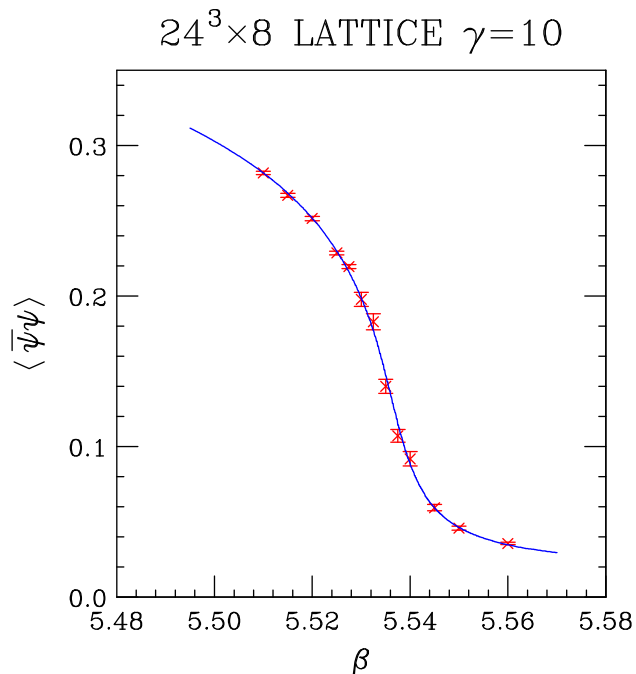


FIG. 18:  $O(2)$  scaling in a finite volume for two flavors of massless staggered fermions with an irrelevant four-fermion interaction, from [67]. The curve comes from an  $O(2)$  spin model simulation with “matched volume”.

depending on where the tricritical point lies, we could (1) encounter a critical point and enter a first order regime, or (2) we may have to go to zero quark mass to find a genuine phase transition. In the right panel we reproduce a result from de Forcrand and Philipsen suggesting the first alternative, but their results were obtained with an unimproved action at  $N_\tau = 4$  for which we expect large cutoff effects.

As we have mentioned, cutoff effects complicate the determination of the phase boundary at small quark mass. This is especially likely to be true for simulations based on unimproved staggered fermions (even improved staggered fermions are not entirely immune), since for them it is important to take the continuum limit before taking the small quark mass limit. Otherwise, one risks being misled by lattice artifacts.

## V. QCD PHASE DIAGRAM AT NONZERO DENSITIES

### A. Phenomenology

As the baryon number density is increased (*i.e.*, all the flavor chemical potentials are increased from zero), according to traditional arguments, there is a chiral-symmetry restoring phase transition along a line in the  $(\mu, T)$  plane when the  $u$  and  $d$  quark masses are zero, as sketched in Fig. 19 [69]. This tradition is founded on two notions. The first argues that asymptotic freedom and consequently deconfinement should reign at very high temperatures and high chemical potential. The second argues that spontaneous chiral symmetry breaking occurs at zero chemical potential because, when fermions acquire a dynamical mass through symmetry breaking, the negative energy levels of the Dirac sea are lowered, lowering the vacuum energy. With a nonzero chemical potential the filled positive energy levels rise in energy, counteracting the advantage of a dynamical chiral mass, and consequently inhibiting spontaneous symmetry breaking [70].

At zero  $u$  and  $d$  quark mass chiral symmetry is exact. If chiral symmetry is restored above a critical chemical potential and it is spontaneously broken below, analyticity requires a phase transition. There are no such guarantees, however, when quark masses are not zero. Since we know from numerical simulation that at physical quark masses there is only a crossover at zero density, the critical line separating the chirally broken from the chirally restored phase must move away from the temperature axis as the quark masses are increased. It then terminates in a critical endpoint  $(T_E, \mu_E)$ . A crossover line then fills the gap from there to the temperature axis, as indicated by the dashed line in Fig. 19. A key phenomenological question is whether the critical endpoint is experimentally accessible.

At still higher densities exotic phases have been proposed, including diquark condensates and color-flavor locked and superconducting phases [72, 73]. These phases are, thus far, completely beyond the reach of current lattice simulations.

### B. Lattice methods for nonzero densities

To confirm or refute these traditional arguments requires numerical simulation. Unfortunately, simulations at nonzero chemical potential are very difficult, since standard lattice methodology requires that the Feynman path integrand be treated as a positive probability measure. In  $SU(3)$  gauge theory, the integrand becomes complex at a nonzero (real) chemical potential. This creates

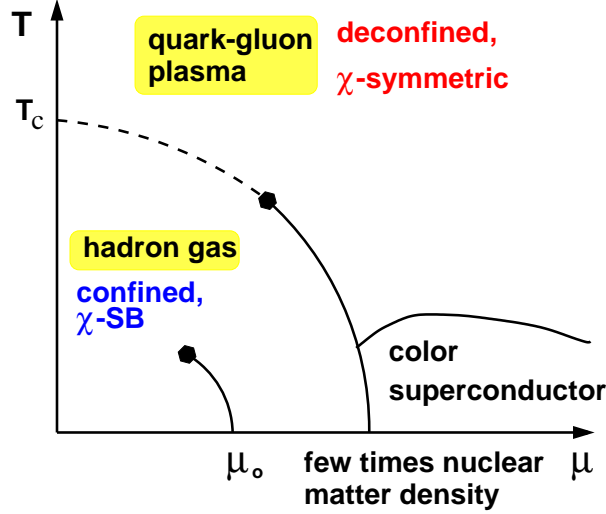


FIG. 19: Sketch of the expected phase diagram for 2+1 flavor hadronic matter as a function of temperature and chemical potential at physical quark masses from [71]. The confined, chiral symmetry broken phase lies in the lower left, separated from the deconfined, chirally symmetric phase by a pseudocritical crossover line (dashed) and first order (solid) line of phase transitions. A critical point is indicated by a black hexagon. A nuclear matter phase transition occurs along a line extending from  $\mu = \mu_0$ . At higher densities a color superconducting phase is proposed.

a fermion “sign problem” analogous to the fermion sign problem in condensed matter physics in strongly-coupled electron systems away from half-filling. A solution to either problem would be beneficial to the other.

To see why the problem arises, consider the naive fermion Dirac matrix  $M(U) = \gamma_v \nabla_v + m$ . The lattice version of the gauge-covariant derivative  $\nabla_v$  is given by Eq. (17). The terms in  $\nabla_v$  in the action allow the quark to hop to next neighbor sites in the positive and negative  $v$  direction. Normally, hopping in all directions must have equal weight to preserve the discrete lattice symmetries of axis interchange, parity, time reversal, and charge conjugation. The fermion determinant is then real because taking its complex conjugate corresponds to reversing the direction of hopping, which has the same weight. But a positive nonzero chemical potential promotes quark hopping in the positive (imaginary) time direction and suppresses it in the negative time direction. This is naturally implemented by changing the covariant time derivative as follows:

$$\nabla_0 \psi(x) \rightarrow \frac{1}{2a} [U_0(x) e^{a\mu} \psi(x + \hat{0}a) - e^{-a\mu} U_0^\dagger(x - \hat{0}a) \psi(x - \hat{0}a)]. \quad (47)$$

If a quark hops along a worldline that wraps completely around the lattice in the imaginary time direction, it accumulates  $N_\tau$  factors of  $\exp(a\mu)$ , and the partition function receives a net enhancement  $\exp(a\mu N_\tau) = \exp(\mu/T)$ , the appropriate statistical weight for the addition of one quark to the grand canonical ensemble. A quark hopping backwards is interpreted as an antiquark, and its contribution is correspondingly suppressed, as it should be. With this imbalance the determinant is no longer guaranteed to be real. Instead it acquires a complex phase  $\phi \propto \mu V$ , *i.e.*, roughly proportional to the lattice volume and the chemical potential.

A complex determinant creates additional problems for staggered fermions. With 2 + 1 flavors of staggered fermions at nonzero densities, one requires the square root and fourth root of the fermion determinants. When the determinant is real, there is no phase ambiguity in the root. But when the determinant is complex, one has to choose the correct Riemann sheet. The ambiguities and an expensive remedy are discussed in [74]. To be safe, one is limited to small  $\mu$  and volumes.

Over the years a number of methods have been proposed for treating a complex determinant. We give a brief account of the attempts. For recent reviews, see [75, 76].

### 1. Reweighting the fermion determinant

As a standard lattice Monte Carlo method, reweighting involves sampling the Feynman path integral according to one measure and then making adjustments to achieve the effect of simulating with a slightly different measure [77, 78].

Let us see how this idea is applied to a simulation at nonzero chemical potentials  $\mu_i$ , one for each flavor  $i$ . (To be precise, we are speaking of a quark-number chemical potential. The baryon-number potential is three times as large ( $\mu_{B_i} = 3\mu_i$ ). The expectation value of an operator  $O$  is given by

$$\langle O \rangle_\mu = \int [dU] O(U) \exp[-S_G(U)] \prod_i \det[M_i(U, \mu_i)] / Z(\mu), \quad (48)$$

where  $\mu = (\mu_1, \mu_2, \dots)$  and

$$Z(\mu) = \int [dU] \exp[-S_G(U)] \prod_i \det[M_i(U, \mu_i)]. \quad (49)$$

Since we can't do importance sampling with the unsuitably complex determinant  $\det[M(U, \mu)]$  in the measure, we can try to do it with the real determinant  $\det[M(U, \mu = 0)]$ . That is, we write

$$\langle O \rangle_\mu = \langle OR(U, \mu) \rangle_0 / \langle R(U, \mu) \rangle_0, \quad (50)$$

where  $R(U, \mu)$  is the ratio of determinants that reweights the contributions to the integrand to compensate for the incorrect sampling measure:

$$R(U, \mu) = \det[M(U, \mu)] / \det[M(U, 0)]. \quad (51)$$

Similarly, we can reweight to imitate a change in any of the parameters of the action including the quark masses and gauge coupling. The reweighting factor  $R$  is simply the ratio of the intended and actual measures.

This procedure, often called the Glasgow method, is mathematically correct but numerically unstable. As the chemical potential moves away from zero, one is no longer doing importance sampling. In complex analysis this approach is similar to attempting to estimate a contour integral in the stationary phase approximation without going through the saddle point. The variance in the sampled values of the numerator and denominator in Eq. (50) grows exponentially as the lattice volume increases, *i.e.*, in the thermodynamic limit. The inevitable breakdown is forestalled by keeping the shift in parameters small, so by working at small  $\mu$ .

A variant of this method uses the absolute value of the determinant for the sample weighting. The reweighting factor is then the phase [79]. This method has been applied only to small lattice volumes.

Fodor and Katz propose reweighting simultaneously in the gauge coupling  $g^2$  and  $\mu$  [80]. They argue that one achieves a better overlap with this method. For example, one might expect that if one moves along the crossover line in the  $\mu - T$  plane, the important integration domain might not change as rapidly as it would if one moves in some other direction. To stay on this line requires changing the gauge coupling along with the chemical potential. To locate the critical line, they follow Lee-Yang zeros of the partition function. (These zeros lie in the complex temperature or complex gauge-coupling plane. If there is a genuine phase transition, as the lattice volume is increased, they impinge on the real temperature axis and give rise to a singularity. If there is only a crossover, they stay harmlessly away from the real axis.) From this method they estimate the critical endpoint at  $T = 160(3.5)$  MeV and  $\mu_B = 3\mu = 360(40)$  MeV at physical quark masses using conventional staggered fermions [81]. This critical chemical potential is nearly a factor of two smaller than an earlier estimate at higher quark masses and smaller volumes [82]. Such sensitivity to the simulation parameters warrants further study.

## 2. *Approximating the determinant with phase quenching*

With degenerate up and down quarks, simulating with the “phase-quenched” or absolute value of the determinant and ignoring the phase completely is equivalent to giving the up quark a positive chemical potential and the down quark a negative chemical potential, so it is equivalent to simulating with an isospin chemical potential [83]. This procedure is numerically tractable, but to draw conclusions regarding the phase diagram with the standard chemical potential requires some justification. Kogut and Sinclair present the case in [84]. See also [85].

## 3. *Simulating in the canonical ensemble*

Another approach is to simulate in the canonical ensemble of fixed quark (baryon) number [86, 87, 88, 89]. For simplicity, consider a single quark species. The canonical ensemble with quark number  $q$  is then obtained from the Fourier transform

$$Z_q = \int_0^{2\pi} d\phi e^{-iq\phi} \int [dU] \exp[-S_G(U)] \det[M(U, \mu)]|_{\mu/T=i\phi}. \quad (52)$$

The sign problem arises in the Fourier transform. As the quark number is increased for a given lattice volume and configuration, the Fourier component decreases rapidly and the sensitivity to oscillations worsens, so that any discrete approximation to the Fourier transform develops a severely large variance.

Meng *et al.* have recently proposed a new “winding number expansion” method that starts from the Fourier transform of the logarithm of the determinant,  $\log(\det[M(U, \mu)]) = \text{Tr} \log[M(U, \mu)]$  and proceeds via a Taylor expansion to generate the canonical partition function [90, 91]. The method converges much better, but so far results are reported only for fairly large quark masses.

## 4. *Simulating with an imaginary chemical potential*

If we make the chemical potential purely imaginary, the fermion determinant becomes real, and a direct simulation is possible [92]. To recover results at a physical, real chemical potential, we must do an analytic continuation. The success of such a continuation depends on knowing the analytic form of the observable as a function of chemical potential. We do if the chemical potential is small enough that a Taylor expansion is plausible. So in the end, the imaginary potential method

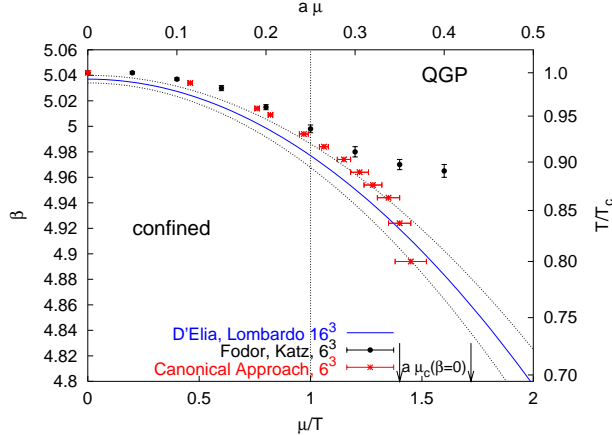


FIG. 20: From [88]. Critical line as a function of quark chemical potential and temperature for four degenerate flavors of unimproved staggered fermions at  $N_\tau = 4$ , bare quark mass  $am = 0.05$ , and for the spatial lattice volumes shown. Results from three methods are compared: the imaginary chemical potential approach of [93], the canonical ensemble approach of [88], and the multiparameter reweighting approach of [80]. A range of strong coupling values of the critical chemical potential  $\mu_c(\beta = 0)$  is also indicated.

provides essentially the same information as an explicit Taylor expansion about zero chemical potential. Figure 20 from de Forcrand and Kratochvila [88] compares three methods for determining the critical line. Each result shown is based on the same unimproved  $N_f = 4$  staggered fermion action. The methods agree reasonably well for  $\mu/T < 1$ . Note that this is a four-flavor simulation with a first-order phase transition, unlike the 2+1-flavor case of Fig. 19.

### 5. Taylor expansion method

For small chemical potential, we may carry out a Taylor expansion of the required observables in terms of the flavor chemical potentials at zero chemical potential [94, 95]. Since all Taylor coefficients are evaluated at zero chemical potential, determining them is straightforward. However, the observables that give the coefficients are nontrivial. They involve products of various traces of the inverse fermion matrix. The traces are usually evaluated using stochastic methods. Furthermore, as the order of the expansion grows, the number of required terms grows factorially. Thus it is rare to find calculations as high as eighth order [96, 97].



## 6. Probability distribution function method

The “probability-distribution-function” or “density-of-states” method is new and promising [98, 99]. It is related to the reweighting method. A recent variant by Ejiri combines reweighting with a Taylor expansion. To explain the method we start with a simple case, defining the “density of states” or “probability distribution function” of the plaquette  $P$  with the Wilson gauge action and arbitrary fermion action:

$$w(P') = \int [dU] \delta(P' - P(U)) \det[M(U, 0)] \exp[-S_G(U)], \quad (53)$$

where  $\delta(P' - P)$  is the Dirac delta function. It is defined like the partition function, but at a fixed value of the plaquette. The expectation value for an observable  $O(P)$  that depends only on  $P$  is then

$$\langle O \rangle = \int dP' w(P') O(P') / \int dP' w(P'). \quad (54)$$

At nonzero  $\mu$  we use reweighting to calculate the partition function:

$$Z(\mu) = \int dP R(P, \mu) w(P), \quad (55)$$

where the plaquette-restricted reweighting function  $R(P, \mu)$  is

$$R(P, \mu) = \frac{\int [dU] \delta(P' - P(U)) \det[M(U, \mu)]}{\int [dU] \delta(P' - P(U)) \det[M(U, 0)]}, \quad (56)$$

*i.e.*, the ratio at nonzero and zero  $\mu$ . For the Wilson action, the gauge weight  $\exp[-S_G(U)]$  depends only on  $P$ , so it cancels between numerator and denominator in  $R(P, \mu)$ . The distribution function  $w(P)$  is still calculated at  $\mu = 0$  according to (53).

The sign problem appears in the numeric evaluation of  $R(P, \mu)$ . Ejiri offers a way to overcome it [99]. His method begins with a generalization of the distribution function, making it depend on three variables: the plaquette  $P$ , the magnitude of the ratio of determinants  $F(\mu) = \det M(\mu) / \det M(0)$ , and the phase  $\theta \equiv \text{Im} \log \det M(\mu)$ :

$$w(P', |F'|, \theta') = \int [dU] \delta(P' - P(U)) \delta(|F'| - |F|) \delta(\theta' - \theta) \det[M(U, 0)] \exp[-S_G(U)], \quad (57)$$

Note that the real, positive weight factor in the integrand comes from the  $\mu = 0$  action. For any value of  $\mu$  the partition function is then

$$Z(\mu) = \int dP d|F| d\theta F(\mu) w(P, |F|, \theta), \quad (58)$$

where in place of the reweighting function  $R$  we now have simply  $F(\mu)$  itself.

The next step relies on the key assumption that the distribution function  $w(P', |F'|, \theta')$  is Gaussian in  $\theta$ . Ejiri argues that this is plausible, at least for large volume. A further assumption for rooted staggered fermions is that the effect on the phase of taking the fourth root is simply to replace  $\theta$  by  $\theta/4$  in the Gaussian distribution. With these assumptions one can do the  $\theta$  integration directly, eliminating the sign problem. The result depends only on the width of the Gaussian, which must be determined numerically. Finally, to make the calculation of the ratio of determinants tractable, Ejiri expands  $\log[\det M(\mu)]$  in a Taylor series in  $\mu$  about  $\mu = 0$ . The same Taylor coefficients appear in an intermediate step in the Taylor expansion of the pressure or thermodynamic potential. Since one is expanding the action instead of the thermodynamic potential, the convergence properties are different — possibly more favorable.

Applying this method to p4fat3 staggered fermions with the Wilson gauge action, a rather coarse lattice with  $N_\tau = 4$ , and a rather large quark mass, Ejiri locates the critical chemical potential at  $\mu/T > 2.5$ , approximately. This is an interesting result, which awaits reconciliation with the questions raised by Golterman, Shamir, and Svetitsky concerning phase ambiguities of the fourth root of the staggered fermion determinant [74].

Thus we see that all of the methods, save, perhaps, the probability distribution function method, are limited to quite small chemical potentials.

### 7. Stochastic quantization method

All of the above lattice methods for simulating at nonzero chemical potential evaluate the Feynman path integral using Monte-Carlo importance sampling, a technique that is inherently unstable when the path integrand is not positive definite. At nonzero chemical potential, the  $SU(3)$  fermion determinant is complex, and the wide variety of methods outlined above deal with the complex phase with limited success. Instead of quantizing via the Feynman path integral method, Aarts and Stamatescu [100] have recently proposed using the stochastic quantization method [101]. In the early days of lattice calculations, stochastic quantization through the Langevin equation [102] was, in fact, one of the competing numerical methods for nonperturbative calculations in quantum field theory, and it met with mixed success [103].

For purposes of this review, we give just a brief sketch of stochastic quantization. For a theory with a scalar field  $\phi(x)$  and action  $S$ , we generate an ensemble of fields  $\phi(x, \tau)$  where  $\tau$  is a

fictitious Langevin time (analogous to molecular-dynamics or Markov-chain time in the standard importance sampling approach.) The ensemble satisfies the stochastic equation

$$\frac{\partial\phi(x,\tau)}{\partial\tau} = -\frac{\delta S}{\delta\phi(x)} + \eta(x,\tau) \quad (59)$$

where  $\eta(x,\tau)$  is a Gaussian random field (source), uncorrelated in  $x$ . As long as  $S$  has a well-defined minimum and we start with a solution near that minimum, without the random source the field relaxes to the classical solution where the action is stationary, *i.e.*, the variational derivative  $\delta S/\delta\phi(x)$  vanishes. The random source then induces “quantum fluctuations” about the classical solution. Quantum observables are estimated in the usual way as expectation values on the equilibrium ensemble.

When the action  $S$  is complex, we get a complex solution and a complex stationary point, a region that is not reached with conventional importance sampling. The hope is that the solution is still attracted to the appropriate stationary point, *i.e.*, the Langevin method is stable. Aarts and Stamatescu have done some preliminary tests with simplified models that imitate the characteristics of QCD at nonzero chemical potential. Their results are promising [104, 105].

### C. Curvature of the critical surface

One question of considerable phenomenological importance can be addressed with simulations at small chemical potential. That is whether the  $Z(2)$  critical line sketched in Fig 14 moves closer to the physical quark masses as the chemical potential is increased or it moves farther away. If it moves closer, as shown in the left panel of Fig. 21, one may expect a true phase transition in a suitably baryon-rich environment, such as may occur in a moderately low-energy heavy-ion collision. If it moves away, as shown in the right panel, there would be no such expectation. De Forcrand and Philipsen set out to address this question using the imaginary chemical potential method. Their results at  $N_\tau = 4$  suggest that the critical line moves away [64, 106, 107, 108], at least when all three quark flavors are close to having equal masses.

## VI. EQUATION OF STATE

The equation of state gives the energy density, pressure, and/or entropy of the thermal QCD ensemble as a function of temperature at constant volume. All quantities are renormalized by

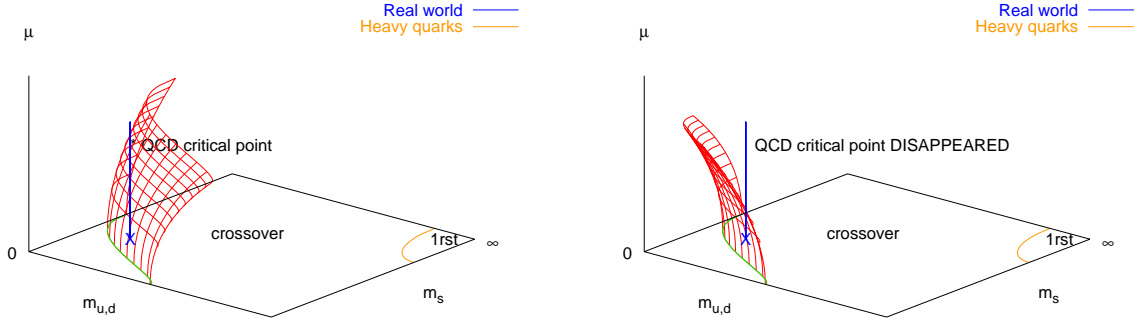


FIG. 21: Two possible alignments of the chiral critical surface at low chemical potential from [64]. Left: the scenario permitting a first order phase transition at high densities and temperatures. Right: the scenario allowing only a crossover.

subtracting their values at zero temperature. The subtraction eliminates an ultraviolet divergence, but the cancellation of this divergence makes the computation costly in the continuum limit, since one must compute the  $O(a^{-4})$  divergent high-temperature and zero-temperature quantities independently and subtract them to get a finite result.

There are two traditional methods for computing the equation of state and one recently introduced method.

### A. Derivative method

The first method is based on the identity

$$\epsilon = \frac{T^2}{V} \left. \frac{\partial \ln Z}{\partial T} \right|_V. \quad (60)$$

On the lattice the derivative with respect to temperature at fixed volume in the first identity translates to a derivative with respect to  $1/(N_\tau a_t)$  at fixed  $a_s$ , where  $a_t$  is the lattice spacing in the imaginary time direction and  $a_s$  is the lattice spacing in the spatial direction. At fixed  $N_\tau$ , we differentiate with respect to  $a_t$  itself.

For example, for the original Wilson plaquette gauge action of Eq. (11) the explicit dependence on  $a_t$  and  $a_s$  goes as follows:

$$S_G(a_s, a_t, g^2) = 2/g^2(a_s, a_t) \left[ \frac{a_s}{a_t} \sum_x P_t(x) + \frac{a_t}{a_s} \sum_x P_s(x) \right], \quad (61)$$

where we have distinguished the timelike and spacelike plaquettes

$$P_t(x) = \sum_i \text{ReTr}[1 - U_{P,i,0}(x)], \quad (62)$$

$$P_s(x) = \sum_{i<j} \text{ReTr}[1 - U_{P,i,j}(x)]. \quad (63)$$

In the gauge action above, we have indicated the dependence of the gauge coupling on the lattice constants  $a_s$  and  $a_t$ . That dependence is defined through a standard renormalization procedure for an anisotropic lattice: at a fixed ratio  $a_t/a_s$  and gauge coupling  $g$ , we compute an experimentally accessible, dimensionful quantity, such as the splitting of a quarkonium system. From the experimental value of the splitting, we can then determine the lattice constants in physical units. We repeat the procedure, varying  $g$  and  $a_t/a_s$  to get the full dependence of  $g$  on the lattice constants.

So from Eq. (15) with only the gauge action in this example, we have [109] (after setting  $a_t = a_s = a$ )

$$\varepsilon = -T \left. \frac{\partial \ln g^2}{\partial \ln a_t} \right|_{a_s} \langle S_G/V \rangle + (6/g^2)T \langle P_t - P_s \rangle. \quad (64)$$

The partial derivative of the gauge coupling with respect to  $a_t$  is called the Karsch coefficient. It is known up to 1-loop order in lattice perturbation theory, but a nonperturbative calculation described above is necessary at experimentally accessible temperatures. As we indicated above, that calculation is rather involved.

## B. Standard integral method

A second thermodynamic identity gives the pressure as the volume derivative of the thermodynamic potential,

$$p = T \left. \frac{\partial}{\partial V} \ln Z \right|_T. \quad (65)$$

By itself, this identity leads to an expression similar to the energy density above, but in this case we need the derivative of the gauge coupling with respect to the spatial lattice spacing  $a_s$  at fixed  $a_t$ . We have the same difficulty as before in requiring a nonperturbative calculation of an unconventional quantity.

But if we combine the two identities to form the interaction measure  $I$ ,

$$I = \varepsilon - 3p, \quad (66)$$

then we get a total derivative of the gauge coupling with respect to  $a = a_s = a_t$  and the lattice thermodynamic identity

$$I = -\frac{T}{V} \frac{d \ln Z}{d \ln a}. \quad (67)$$

The isotropic derivative of the coupling with respect to the cutoff is just the commonly computed renormalization group beta function  $\beta = dg^2/d \ln a$ . For the Wilson plaquette gauge action we get

$$I = -T/V (d \ln g^2 / d \ln a) \langle S_G \rangle. \quad (68)$$

So the lattice derivative is readily calculated in terms of the conventional plaquette observable and the beta function. With fermions present we require also the chiral condensate and the derivative of the quark masses with respect to the lattice spacing. These are also easily accessible in lattice calculations.

We must bear in mind that the physical quantities require subtracting the zero-temperature values, so in the end we need the difference

$$\Delta I = I(T) - I(0). \quad (69)$$

We will often drop the  $\Delta$  in the following discussion and figures.

Figure 22 shows the interaction measure difference obtained in a recent  $N_\tau = 8$  calculation with equal-mass up and down quarks and a strange quark. The mass of the strange quark was held fixed at approximately its physical value, and the masses of the up and down quarks were set to a fixed fraction of the strange quark mass. Thus the temperature was varied roughly along parameter-space lines of constant physics, meaning light pseudoscalar mesons (at zero temperature) had approximately constant masses.

To complete the determination of the equation of state, we need the energy density and pressure separately. The pressure is easily computed in the thermodynamic limit, in which  $\ln Z$  is simply proportional to the volume:

$$\ln Z = -pV/T, \quad (70)$$

So the expression (67) can also be written as

$$I = \frac{T}{V} \frac{d(pV/T)}{d \ln a}, \quad (71)$$

or, if we fix  $VT^3$  in the derivative, as

$$I/T^4 = \frac{d(p/T^4)}{d \ln T}. \quad (72)$$

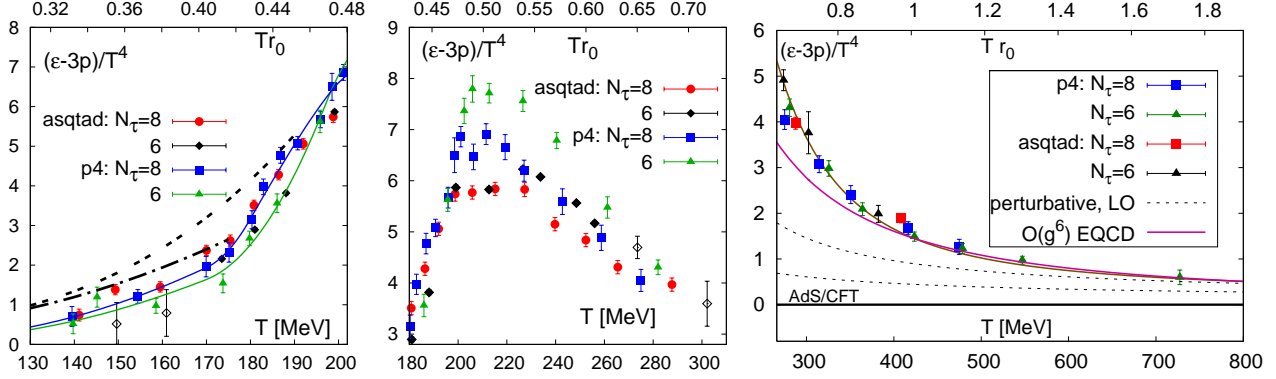


FIG. 22: Details of the dependence of the interaction measure on temperature in MeV units (bottom scale) and  $r_0$  units (top scale) for three temperature ranges left to right: low, middle, and high, for  $N_\tau = 6$  and 8 from a HotQCD study comparing p4fat3 and asqtad staggered fermion formulations [51, 110]. Measurements in most cases are taken along a line of constant physics with  $m_{ud} = 0.1m_s$ . In the low temperature range the dashed and dash-dotted curves are predictions of a hadron resonance gas model with different high mass cutoffs. The other curves in that range are spline fits to the data. In the high temperature range the dashed lines are the leading order perturbative prediction for  $\mu_{\overline{MS}} = 2\pi T$  and  $\mu_{\overline{MS}} = \pi T$ . The brown line (the line passing through the points) is a fit to leading order perturbation theory plus a bag constant, and the magenta line (the line passing mostly below the points) is an  $O(g^6)$  EQCD prediction from [111]. For a brief mention of EQCD, see Sec. VII A.

We can then use the identity (71) at fixed  $N_\tau$  to integrate with respect to  $\ln a$  (equivalently  $\ln T$ ) to get the pressure:

$$p(a)a^4 - p(a_0)a_0^4 = - \int_{\ln a_0}^{\ln a} \Delta I(a')(a')^4 d \ln a'. \quad (73)$$

Here the lower endpoint of integration  $a_0$  is a large lattice spacing, corresponding to a low temperature. If it is sufficiently low, we may take  $p(a_0) = 0$  and the expression then yields the pressure at temperature  $T = 1/(N_\tau a)$ .

The integration is carried out numerically, since the integrand is determined in a series of simulations done at fixed lattice spacing. However, the spacing of the points can be set arbitrarily close as needed. The energy density is then obtained from  $\varepsilon = I + 3p$  and the entropy density from  $s = \varepsilon + p$ .

This integral method was used to complete the construction of the equation of state with improved staggered quarks shown in Fig. 23. The same method has also been used in a study with two flavors of clover improved Wilson fermions [112], as shown in Fig. 24.

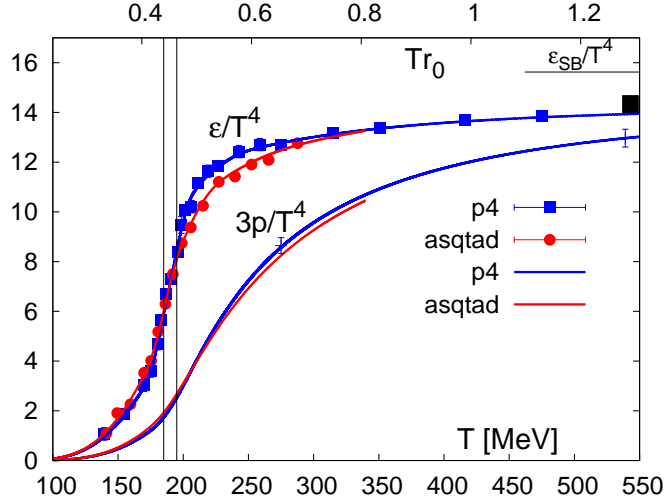


FIG. 23: Equation of state showing energy density and three times the pressure, both divided by the fourth power of the temperature vs. temperature for  $N_\tau = 8$ . Measurements are taken along a line of constant physics with  $m_{ud} = 0.1m_s$ . Results are from a HotQCD study comparing p4fat3 and asqtad staggered fermion formulations [51]. The blue error bars on the pressure curve indicate the size of the error. The black bar shows a systematic error from setting the lower limit of the pressure integration.

### C. Temperature integral method

In the standard integral method above we fixed  $N_\tau$  and integrated Eq. (67) with respect to lattice spacing to get the pressure. The temperature integral method of [113] instead fixes the lattice spacing and “integrates” Eq. (72) over  $N_\tau$  at fixed  $N_s$ .

The advantage of working at a fixed lattice spacing (so fixed gauge coupling, quark masses, and Hamiltonian) is that the zero temperature subtraction is the same for all  $N_\tau$ , and we are assured of following lines of constant physics [114]. With the standard integral method, to carry out the necessary subtraction, we need a separate zero temperature simulation for each high temperature point. Thus one may hope for a savings in computational effort.

The disadvantage of the temperature integral method is that the integrand is known only at the discrete temperatures  $1/(N_\tau a_t)$  for integer  $N_\tau$ . To decrease the sample interval at a given temperature, one must start with a smaller  $a_t$ , which increases the cost substantially. Simulating on an anisotropic lattice helps.

So far, the method has been tested on a pure Yang-Mills ensemble with the pleasing result shown in Fig. 25.



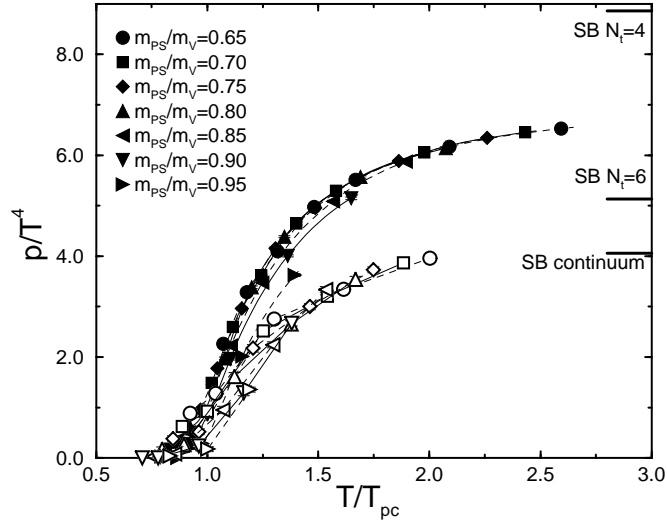


FIG. 24: The pressure as function of  $T/T_{pc}$ , with  $T_{pc}$  the pseudocritical or crossover temperature for two-flavors of clover improved Wilson fermions on  $16^3 \times 4$  lattices (filled symbols) and  $16^3 \times 6$  lattices (open symbols), from [112]. The simulation was done for a variety of rather heavy quark masses, indicated by the vector to pseudoscalar mass ratios  $m_{PS}/m_V$ . The lattice artifacts are larger than with improved staggered quarks, as expected from Table I.

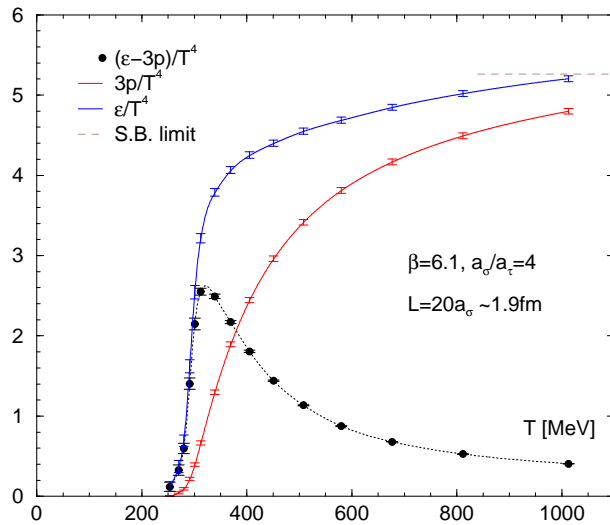


FIG. 25: Equation of state (interaction measure, energy density and pressure) for pure Yang-Mills theory, obtained using the  $T$  integral method at fixed lattice spacing  $a_\sigma = 0.097$  fm and aspect ratio  $a_\sigma/a_\tau = 4$  [113, 115].

#### D. Step scaling method

The standard integral method of Eq. (73) has the disadvantage that it requires computing the difference between the high and zero temperature values of the interaction measure at each value of the gauge coupling (*i.e.*, each high temperature point). At increasingly high temperature we get closer to the continuum limit and the matching zero temperature calculation becomes very expensive. Endrödi *et al.* propose a step scaling method that alleviates this problem to some degree [116]. Their idea is to compute the pressure at a given temperature as a series of differences:

$$p(T) - p(0) = [p(T) - p(T/2)] + [p(T/2) - p(T/4)] + \dots \quad (74)$$

The increment

$$\bar{p}(T) = p(T) - p(T/2) \quad (75)$$

must be calculated at the same cutoff  $a$  to renormalize properly the ultraviolet divergence. In practice, this means matching a calculation at a given  $N_\tau = N$  with a calculation at  $N_\tau = 2N$  for the same bare action parameters. (The step factor 1/2 can be replaced by any factor less than 1.) The differences  $[p(T) - p(T/2)]/T^4$  are bounded from above, so the series

$$[p(T) - p(0)]/T^4 = \bar{p}(T)/T^4 + \frac{1}{16}\bar{p}(T)/T^4|_{T/2} + \frac{1}{256}\bar{p}(T)/T^4|_{T/4} + \dots \quad (76)$$

converges rapidly.

Endrödi *et al.* suggest two ways to calculate  $\bar{p}(T)$ . One uses a modified form of Eq. (73).

$$p(a, N_\tau = N)a^4 - p(a, N_\tau = 2N)a^4 = - \int_{\ln a_0}^{\ln a} [I(a', N_\tau = N) - I(a', N_\tau = 2N)](a')^4 d \ln a'. \quad (77)$$

Here, we have shown the  $N_\tau$  dependence explicitly. We assume that  $a_0$  is large enough that the integration constants  $p(a_0, N_\tau)$  are essentially zero.

The second method uses the identity Eq. (70) to write

$$\bar{p}(T = 1/(aN)) = p(a, N_\tau = N) - p(a, N_\tau = 2N) = [\ln Z(N_\tau = 2N) - \ln Z^2(N_\tau = N)]/(N_s^3 N). \quad (78)$$

The rhs is the difference between the partition functions on two lattices of size  $N_s^3 \times 2N$  in which one lattice is intact and the other is split in half at the midpoint in imaginary time with periodic (or fermion-antiperiodic) boundary conditions applied to the two halves. To compute this difference, Endrödi *et al.* modify the action at the interface by introducing an interpolating parameter  $\alpha$  such that  $\alpha = 1$  corresponds to the fully split lattice and  $\alpha = 0$ , to the fully intact lattice. The simulation

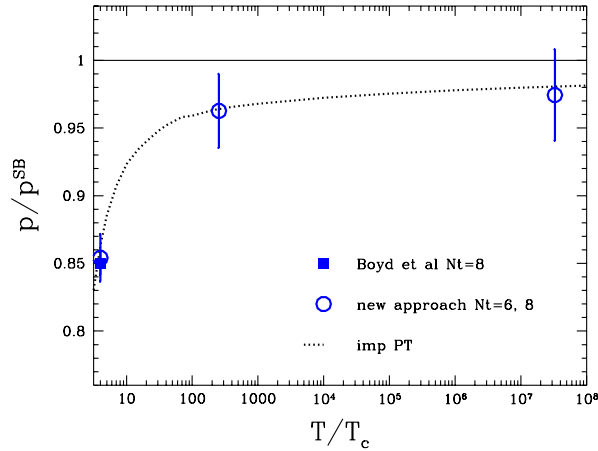


FIG. 26: Circles: pressure from [116] for pure Yang-Mills theory at ultra-high temperatures compared with predictions of EQCD perturbation theory (dotted line [111, 117, 118]). The pressure is given in units of the Stefan-Boltzmann value and the temperature in units of the temperature at the phase transition  $T_c$ . The square is computed using the standard integral method [119].

measures the derivative of  $\ln Z(\alpha)$  with respect to  $\alpha$ , which involves only fields at the interface. The increment (78) is then computed from

$$\bar{p}(T) = \frac{1}{N_s^3 N} \int_0^1 d\alpha \frac{d \ln Z(\alpha)}{d\alpha}. \quad (79)$$

There is still a strong cancellation involved in the integration over  $\alpha$ , but it is a bit milder than the cancellation in the standard integral method. With their method they are able to reach such high temperatures that contact with perturbation theory is certainly expected, as shown in Fig. 26. For a lower temperature comparison of the  $O(g^6)$  EQCD prediction of Laine *et al.* [111] with the interaction measure computed using standard methods, see Fig. 22. For a brief mention of EQCD, see Sec. VII A.

### E. Equation of state at nonzero densities

Heavy ion collisions involve interacting hadronic matter at relatively low baryon densities and high temperatures. At the other extreme, high baryon densities and low temperatures may occur in the cores of dense stars. In both cases we would like to know the equation of state. For the

low density environment of heavy ion collisions the Taylor series method is effective for lattice simulations. Unfortunately, thus far we have no reliable lattice method to simulate the conditions of dense stars.

Consider the  $2 + 1$  flavor case of equal nonzero up- and down-quark chemical potentials  $\mu_u = \mu_d = \mu_{ud}$  and a nonzero strange chemical potential  $\mu_s$ . The pressure can be expanded as follows:

$$\frac{P}{T^4} = \sum_{n,m=0}^{\infty} c_{nm}(T) \left(\frac{\mu_{ud}}{T}\right)^n \left(\frac{\mu_s}{T}\right)^m, \quad (80)$$

The coefficients  $c_{nm}$  are evaluated at zero chemical potential

$$c_{nm}(T) = \frac{1}{n!} \frac{1}{m!} \frac{1}{T^3 V} \frac{\partial^{n+m} \ln Z}{\partial (\mu_{ud}/T)^n \partial (\mu_s/T)^m} \Big|_{\mu_{ud,s}=0}. \quad (81)$$

CP symmetry requires that the coefficients vanish for odd  $n + m$  at zero chemical potential.

For increasing  $n$  and  $m$  the coefficients  $c_{nm}$  are increasingly complicated combinations of traces of the inverse of the lattice Dirac matrix. For a simple example, the lowest order mixed coefficient is

$$c_{11} = \left\langle \text{Tr} \left( M_{ud}^{-1} \frac{\partial M_{ud}}{\partial (\mu_{ud}/T)} \right) \text{Tr} \left( M_s^{-1} \frac{\partial M_s}{\partial (\mu_s/T)} \right) \right\rangle. \quad (82)$$

Such observables are technically difficult to compute because the trace is over all lattice sites as well as over colors. Usually such traces are evaluated by stochastic sampling methods. As the order  $n$  and  $m$  increase, not only are the traces more complicated, the required number of stochastic samples grows rapidly. In effect, the computational effort grows factorially in the expansion order.

The quark number densities  $\langle n_{ud} \rangle$  and  $\langle n_s \rangle$  can be found from first derivatives in the same expansion. For  $\langle n_{ud} \rangle$  it is

$$\langle n_{ud} \rangle = \frac{1}{V} \frac{\partial \ln Z}{\partial (\mu_{ud}/T)} = T^3 \sum_{n=1, m=0}^{\infty} n c_{nm}(T) \left(\frac{\mu_{ud}}{T}\right)^{n-1} \left(\frac{\mu_s}{T}\right)^m, \quad (83)$$

and for  $\langle n_s \rangle$ ,

$$\langle n_s \rangle = \frac{1}{V} \frac{\partial \ln Z}{\partial (\mu_s/T)} = T^3 \sum_{n=0, m=1}^{\infty} m c_{nm}(T) \left(\frac{\mu_{ud}}{T}\right)^n \left(\frac{\mu_s}{T}\right)^{m-1}. \quad (84)$$

The leading terms in the expansion are

$$\frac{\langle n_s \rangle}{T^3} \approx c_{11}(T) \left(\frac{\mu_{ud}}{T}\right) + c_{02}(T) \left(\frac{\mu_s}{T}\right). \quad (85)$$

The mixed coefficient  $c_{11}(T)$  is nonzero (and negative) at low temperatures, because when we add a strange quark to the ensemble, it is screened by a light antiquark. This tendency persists at temperatures close to, but above the crossover. So for  $\mu_{ud} \neq 0$ , the strange quark number density

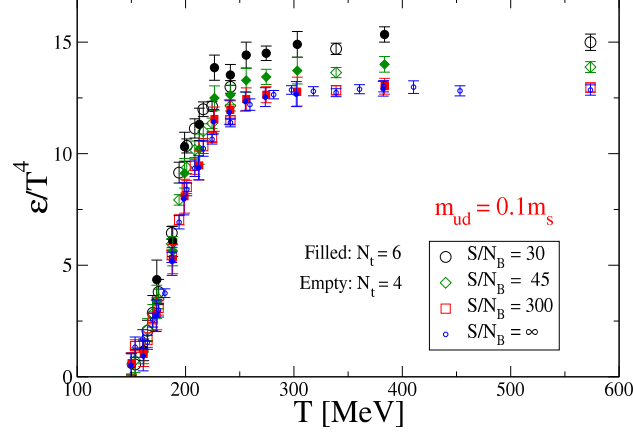


FIG. 27: Energy density vs temperature for constant entropy per baryon number, from [121].

is nonzero for  $\mu_s = 0$ . In heavy ion collisions the mean strange quark number density is zero, so we need to “tune” the strange quark chemical potential to obtain the experimental conditions.

The quark number susceptibility matrix  $\chi_{ab}$  for  $a, b \in u, d, s$  is likewise found from second derivatives. For example, for the diagonal elements and the equivalent mixed light off-diagonal elements  $\chi_{uu} = \chi_{dd} = \chi_{ud} = \chi_{du}$ , we have

$$\chi_{uu} = \frac{\partial \langle n_{ud}/T \rangle}{\partial (\mu_{ud}/T)} = T^2 \sum_{n=2, m=0}^{\infty} n(n-1) c_{nm}(T) \left( \frac{\mu_{ud}}{T} \right)^{n-2} \left( \frac{\mu_s}{T} \right)^m. \quad (86)$$

The (diagonal) strange quark number susceptibility  $\chi_s = \chi_{ss}$  is similarly obtained. The heavy-light mixed quark number susceptibility  $\chi_{us} = \chi_{su}$  is

$$\chi_{us} = \frac{\partial \langle n_{ud}/T \rangle}{\partial (\mu_s/T)} = T^2 \sum_{n=1, m=1}^{\infty} n m c_{nm}(T) \left( \frac{\mu_{ud}}{T} \right)^{n-1} \left( \frac{\mu_s}{T} \right)^{m-1}. \quad (87)$$

The interaction measure can also be expanded in this way [120]. Once we have both pressure and interaction measure, we can determine the energy density and entropy density for any small chemical potential. As an example, we show the equation of state at constant entropy density per baryon number in Fig. 27. This is the equation of state appropriate to an adiabatic expansion or compression of hadronic matter, conditions that may obtain in a heavy ion collision.

## VII. IN-MEDIUM PROPERTIES OF HADRONS

### A. Spatial string tension

Despite its popular characterization as deconfined, high-temperature hadronic matter retains vestiges of confinement. Space-like Wilson loops still exhibit the area-law behavior associated with confinement. This is readily seen by considering dimensional reduction, in which for  $T \gg T_c$ , the short Euclidean time dimension (of extent  $1/T$ ) is collapsed, leaving three spatial dimensions [122, 123]. Since all dimensions are Euclidean, any one of them can be interpreted as Euclidean “time.” We do a  $90^\circ$  rotation to turn one of the original spatial coordinates into the Euclidean time coordinate of a 2+1 dimensional field theory.

The reduction of 4-d QCD to what is sometimes called “EQCD” [117] has these characteristics:

- Quarks acquire a large 3-d mass  $\sqrt{(\pi T)^2 + m_q^2}$ . This happens because the antiperiodic boundary condition in the small dimension requires a minimum momentum component  $\pi T$  for that coordinate, which then contributes to the energy-momentum relation as an additional effective mass.
- The original fourth component of the color vector potential  $A_0$  is reinterpreted as a scalar Higgs-like field. The other three vector potential components become the usual vector potential of the 2+1 dimensional theory. We get a confining gauge-Higgs theory.
- The 3-d and 4-d gauge couplings are related through  $g_3 = g_4\sqrt{T}$ .
- The spatial Wilson loop of the original 4-d theory is now interpreted as the standard space-time-oriented Wilson loop of the 3-d theory. Because the theory is still confining in 3-d, we get a linearly rising potential with a string tension.

In a recent calculation Cheng *et al.* compared the behavior of the spatial string tension of the full 4-d theory with predictions based on a perturbative connection between the four- and three-dimensional coupling and the numerically measured proportionality between string tension and coupling in three-dimensional  $SU(3)$  Yang-Mills theory [124]. The comparison is shown in Fig. 28. The good agreement at temperatures as low as  $1.5T_c$  is unexpected.

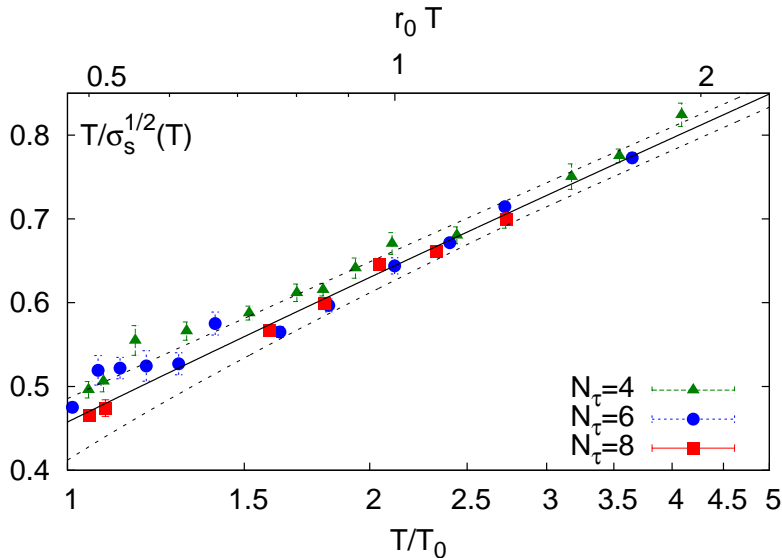


FIG. 28: Temperature divided by the square root of the spatial string tension  $\sigma_s$  vs. temperature in units of the crossover temperature  $T_0$  (lower scale) and in  $r_0$  units (upper scale) for  $2 + 1$  flavors of p4fat3 quarks on lattices with  $N_\tau = 4, 6$  and  $8$ . The solid curve (with uncertainties indicated by the dashed lines) is the prediction of the dimensionally reduced theory [124]

## B. Screening masses

The Yukawa potential can be thought of as a measure of the spatial correlation of a pion source and sink (the sources and sinks being static nucleons). The important insight here is that the screening mass  $m_\pi$  is the mass of a propagating particle. In the high temperature plasma we can consider similar correlations between interpolating operators of any type. These spatial correlators are controlled by confined states, as we indicated in Sec. VII A. Because we no longer have Lorentz invariance, the spatial screening masses are not expected to be equal to frequencies of real-time plasma excitations, but one can speculate that there may be a connection [125]. In any case, they provide information about the structure of the plasma, they control the behavior of a variety of susceptibilities, and their degeneracy patterns provide information about the temperature dependence of symmetries.

Euclidean thermal hadron propagators (correlators) are defined in the same way as they are at

zero temperature:

$$C_{AB}(x) = \langle O_A(x)O_B(0) \rangle, \quad (88)$$

where  $O_A(x)$  and  $O_B(x)$  are interpolating operators for the desired hadronic state.

At zero temperature it is typical to project the correlator to zero spatial momentum, resulting in a time-slice correlator

$$C_{AB}(t) = \int d^3\mathbf{x} C_{AB}(t, \mathbf{x}). \quad (89)$$

At large Euclidean time such a correlator has the asymptotic behavior

$$C_{AB}(t) \sim Z_A Z_B \exp(-Mt), \quad (90)$$

where  $M$  is the mass of the hadron and  $Z_A$  and  $Z_B$  are overlap constants.

At nonzero temperatures one cannot explore the asymptotic limit because of the bound on Euclidean time  $0 \leq t \leq 1/T$ , but one can define a spatial correlator by fixing one of the spatial coordinates and integrating over the other three, as in

$$C_{AB}(z) = \int dt dx dy C_{AB}(t, x, y, z). \quad (91)$$

(For fermions, it is necessary to include a Matsubara phase factor  $\exp[i\pi T t]$ .) For large  $z$  the asymptotic behavior is

$$C_{AB}(z) \sim Z_A(T) Z_B(T) \exp[-\mu(T)z], \quad (92)$$

where  $\mu(T)$  is the hadronic screening mass. At zero temperature  $\mu(T=0) = M$ .

Even though the high-temperature plasma exhibits deconfining characteristics in its real time behavior, the spatial correlations remain confined, so the spectrum of spatial meson and baryon screening masses retains a gap characteristic of confinement even in the high-temperature plasma. However, since the screening mass for quarks approach  $\pi T$  at high temperatures, the valence-quark-antiquark meson screening masses approach  $2\pi T$  and the valence-three-quark baryon screening masses approach  $3\pi T$ . Furthermore, as chiral symmetry is approximately restored at high temperatures, they must exhibit the approximate degeneracies required by the chiral multiplets.

Armed with this background let us consider the temperature behavior of the screening mass  $\mu_\pi(T)$  of the pion. At low temperatures the pion is a Goldstone boson, so the screening mass is small. Above the transition chiral symmetry is restored. So the screening mass rises above the transition temperature, approaching  $2\pi T$ . The transition temperature is marked by the change of slope. Figure 29 illustrates this behavior.



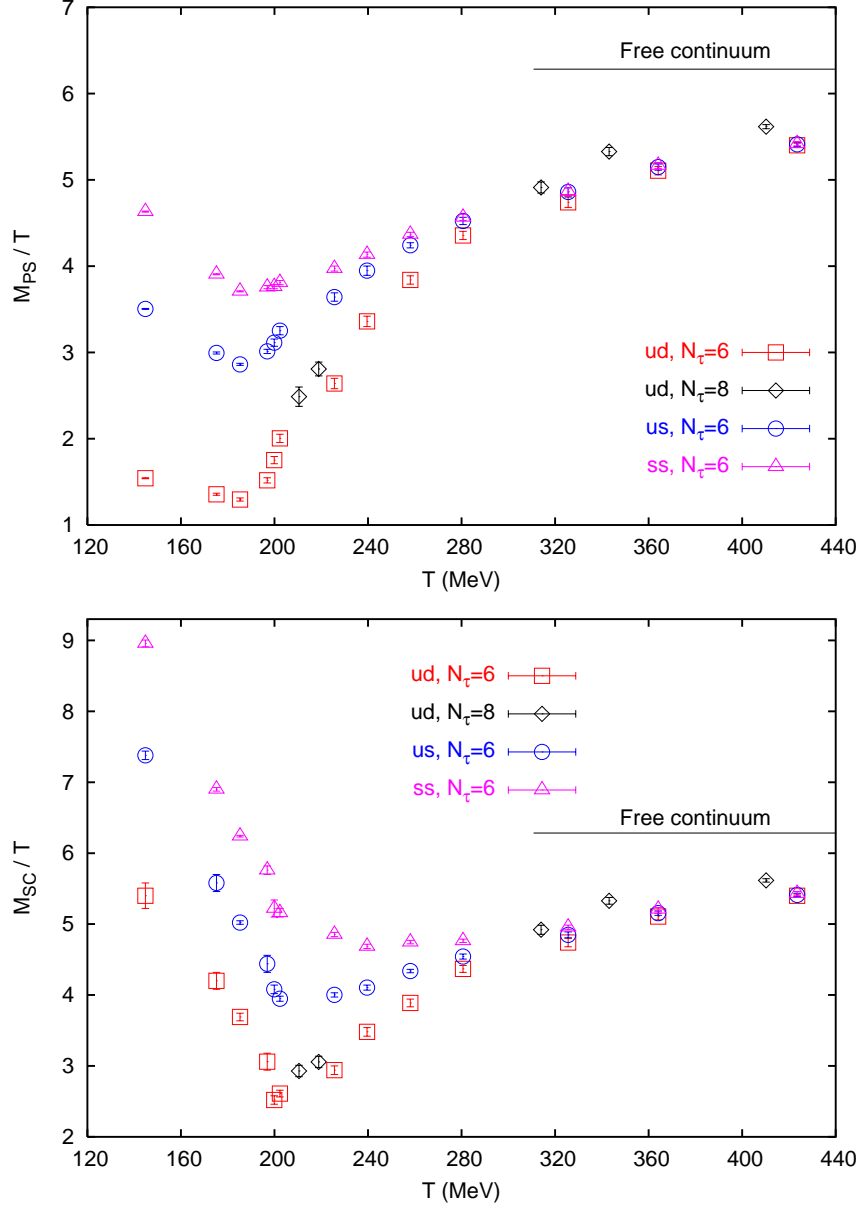


FIG. 29: Screening masses for the pseudoscalar channel (upper panel) and scalar channel (lower panel) vs. temperature in a dynamical 2 + 1 flavor simulation with p4fat3 staggered fermions [126]. Measurements were taken along lines of constant physics with  $m_\pi \sim 220$  MeV,  $m_K = 500$  MeV and  $N_\tau = 6$  and 8 [127].

The isosinglet scalar  $f_0$  ( $\sigma$ ) meson can be generated using the isosinglet chiral condensate  $\bar{\Psi}\Psi_{\text{sing}} = \bar{\Psi}\Psi_u + \bar{\Psi}\Psi_d$  as the interpolating operator. It has a sizable mass at low temperature, but it joins the pion chiral multiplet at the transition temperature when the pion screening mass is quite small. Thus its mass must dip at the transition temperature and rise again, approaching  $2\pi T$ . Thus

a dip in  $\mu_{f_0}$  also marks the transition temperature.

The chiral susceptibilities are related to hadron propagators in Euclidean space-time. For example, the isosinglet chiral susceptibility is

$$\chi_{\text{sing}}(T) = \int d^4x \langle \bar{\psi} \psi_{\text{sing}}(x) \bar{\psi} \psi_{\text{sing}}(0) \rangle = \int dz C_{\text{sing}}(z, T), \quad (93)$$

where  $C_{\text{sing}}(z)$  is the scalar-isosinglet screening correlator generated by the isosinglet chiral condensate. In addition to the  $f_0$ , this correlator also contains a two-pion continuum contribution. So its asymptotic behavior has terms in  $\exp(-\mu_{f_0}z)$  as well as  $\exp(-2E_\pi z)$  for  $E_\pi \geq \mu_\pi$ . Integration over  $z$  of these asymptotic terms yields contributions to the susceptibility that go as the inverse of the screening masses. At low temperatures the two-pion threshold is below the  $f_0$ , so the two-pion continuum dominates the susceptibility. In the chiral limit this contribution is responsible for the  $1/\sqrt{m}$  singularity in the susceptibility. At high temperatures the pion screening mass rises, and the  $f_0$  screening mass is approximately degenerate with it. Thus the two-pion continuum is expected to have a higher screening mass than the  $f_0$ , and the susceptibility is finite in the chiral limit. Thus this susceptibility should be large at low temperatures and fall abruptly at the transition temperature.

### C. Charmonium

To the extent the transition to a quark-gluon plasma is a crossover and not a genuine phase transition, one should not expect low temperature properties to change abruptly at the crossover temperature. Confined hadronic states may persist as plasma excitations at least for temperatures close to, but above the crossover temperature. One of the most studied examples is the  $J/\psi$ , since it is readily observed experimentally, and, because of their large mass, charmed quarks are a good theoretical probe. Numerical simulation suggests that the  $J/\psi$  persists to temperatures as high as  $1.5T_c$  [128, 129]. (See Sec. VII C 3 below.) As the temperature increases beyond  $T_c$ , it is thought that screening of the heavy-quark potential eventually prevents the formation of a bound state and  $J/\psi$  production is suppressed [129, 130].

#### 1. Static quark/antiquark free energy

There are two lattice methods for studying thermal effects in quarkonium. The first, more model-dependent method, is based on a Born-Oppenheimer approximation [130]. One measures

the free energy of a static quark-antiquark pair as a function of separation  $r$ . The result is introduced into the Schrödinger equation as a temperature-dependent potential  $V(r, T)$  for a given heavy quark mass. As the temperature increases, screening effects weaken the potential, and eventually it does not support a bound state for quarks of the given mass. This approximation should be good, provided the Born-Oppenheimer adiabatic approximation is good, *i.e.*, as long as the plasma is able to relax to its equilibrium state on the time scale of the orbital motion of the quarks.

Gauge invariance presents a subtlety in fashionable methods for extracting the free energy to be used as a Born-Oppenheimer potential. It is popular to distinguish between color-singlet and color-octet states of the static quark and antiquark. Since those states are supposed to be defined in terms of the colors of only the spatially separated quarks themselves, the separation is gauge dependent and probably not phenomenologically significant [131].

The potential method can be tested entirely in the context of a lattice calculation. One starts from the lattice static potential, derives the spectral function for the thermal quarkonium propagator (see the next subsection), and compares the result with a direct determination of the lattice spectral function. If the static approximation is correct, the results should agree. Recent attempts to follow this approach for  $T_c < T < 1.5T_c$  fail to reproduce any charmonium states in the spectral function nor any but the 1S state of bottomonium [132]. So is the determination of the lattice spectral function unreliable, or is the static approximation unreliable for charmonium, or are both unreliable?

Related attempts have been made to derive a heavy-quark potential suitable for use in the Schrödinger equation in real time (as opposed to lattice imaginary time), but so far the methodology is developed only in perturbation theory [133, 134, 135].

## 2. Spectral density

The second method is model independent, but more difficult. One measures the spectral function of a thermal Green's function for the  $J/\psi$  [136]. The correlator is defined for some suitable local interpolating operator  $O(x_0, \mathbf{x})$  as

$$C(x_0, \mathbf{x}, T) = \langle O(x_0, \mathbf{x}) O(0, 0) \rangle. \quad (94)$$

The spectral density  $\rho(\omega, \mathbf{q}, T)$  is then obtained by inverting the Kubo formula for the partial Fourier transform  $C(x_0, \mathbf{q}, T)$  of the correlator:

$$C(x_0, \mathbf{q}, T) = \frac{1}{2\pi} \int_0^\infty d\omega \rho(\omega, \mathbf{q}, T) K(\omega, x_0, T), \quad (95)$$

where

$$K(\omega, x_0, T) = \frac{\cosh \omega(x_0 - 1/2T)}{\sinh(\omega/2T)}. \quad (96)$$

Going from the Euclidean correlator  $C(x_0, \mathbf{q}, T)$  to the spectral density  $\rho(\omega, \mathbf{q}, T)$  is a very difficult inverse problem. One would like to extract detailed information about the spectral density from quite limited information. Because of time-reflection symmetry, a simulation at  $N_\tau = 8$  has only five, typically noisy, independent values.

Possible remedies include (1) assuming a functional form for  $\rho$  and fitting its parameters (*e.g.*, a delta function for the  $J/\psi$  or a Breit-Wigner shape), (2) decreasing the time interval  $a_t$ , allowing a larger  $N_\tau$ , and (3) adding further constraints on  $\rho$ , as in the maximum entropy method. We outline the last remedy in the next subsection.

### 3. Maximum entropy method

The maximum entropy method has been used to determine spectral functions in condensed matter physics for some time [137]. It was first applied to lattice QCD by Asakawa, Hatsuda, and Nakamura [138, 139]. It is essentially a Bayesian method with a prior inspired by Occam's razor. One begins by defining an unremarkable default prior spectral density  $\rho_0(\omega, T)$ . A typical choice would be the spectral density of a noninteracting quark-antiquark pair, or at least the density expected at asymptotically high frequency. One then requires that the spectral density  $\rho$ , inferred from the correlator data, should deviate only as much from  $\rho_0$  as the data seems to require.

The method is applied in the context of a maximum-likelihood fit to the correlator data. We give a simplified description of the method. Starting from a parameterization of the spectral density  $\rho(\omega, T)$ , one predicts the correlator data and computes the usual chisquare  $\chi^2[\rho]$  difference between prediction and data. One introduces a Shannon-Jaynes entropy for this  $\rho$  as follows

$$S[\rho] = \int_0^\infty d\omega [\rho(\omega) - \rho_0(\omega) - \rho(\omega) \ln[\rho(\omega)/\rho_0(\omega)]]. \quad (97)$$

The ‘‘entropy’’ vanishes when  $\rho = \rho_0$  and for small deviations from  $\rho_0$ , it is

$$S[\rho] \approx -\frac{1}{2} \int_0^\infty d\omega [\rho(\omega) - \rho_0(\omega)]^2 / \rho_0(\omega). \quad (98)$$

So the default prior maximizes the entropy. One then maximizes the likelihood  $\exp(Q[\alpha, \rho])$  or, equivalently,  $Q[\alpha, \rho]$  itself:

$$Q[\alpha, \rho] = \alpha S[\rho] - \chi^2[\rho]/2. \quad (99)$$

The positive weight  $\alpha$  controls the balance between maximum entropy and minimum chisquare. In the “state-of-the-art” method, the mean of the best fits  $\bar{\rho}$  is then obtained from the average:

$$\bar{\rho} = \int d[\rho] d\alpha \exp(Q[\alpha, \rho]). \quad (100)$$

This is our answer for the spectral density.

This method was used by Asakawa and Hatsuda to study the fate of charmonium in the high-temperature medium [128]. See also [129] and, more recently, [140]. Their results for the  $J/\psi$  spectral density are shown in Fig. 30 and provided some of the first evidence that the  $J/\psi$  exists as a discernible plasma resonance for temperatures at least as high as  $1.62T_c$  before it “melts.”

When data are inadequate, results of the MEM method can be quite sensitive to the choice of the default model. For example, one may obtain artifact excited state peaks. For some examples, see [141].

## VIII. TRANSPORT COEFFICIENTS

### A. Shear and bulk viscosities

Among the transport coefficients, the shear and bulk viscosities are essential to the hydrodynamical modeling of the expansion and cooling of the quark-gluon plasma in the aftermath of a heavy ion collision. They are obtained from correlators of the energy-momentum tensor at temperature  $T$

$$C_{\mu\nu, \rho\sigma}(x_0, \mathbf{x}, T) = \langle T_{\mu\nu}(x_0, \mathbf{x}) T_{\rho\sigma}(0) \rangle. \quad (101)$$

We need its spectral function  $\rho$ , which we obtain from its partial Fourier transform  $C_{\mu\nu, \rho\sigma}(x_0, \mathbf{q}, T)$  and the Kubo formula

$$C_{\mu\nu, \rho\sigma}(x_0, \mathbf{q}, T) = \int_0^\infty d\omega \rho_{\mu\nu, \rho\sigma}(\omega, \mathbf{q}, T) K(\omega, x_0, T), \quad (102)$$

where  $K(\omega, x_0, T)$  is given by Eq. (96). The shear ( $\eta$ ) and bulk ( $\zeta$ ) viscosities are obtained from the low-frequency behavior of the spectral function  $\rho(\omega, \mathbf{q}, T)$ :

$$\eta(T) = \pi \lim_{\omega \rightarrow 0} \frac{\rho_{12, 12}(\omega, 0, T)}{\omega}, \quad \zeta(T) = \frac{\pi}{9} \lim_{\omega \rightarrow 0} \frac{\rho_{ii, jj}(\omega, 0, T)}{\omega}. \quad (103)$$

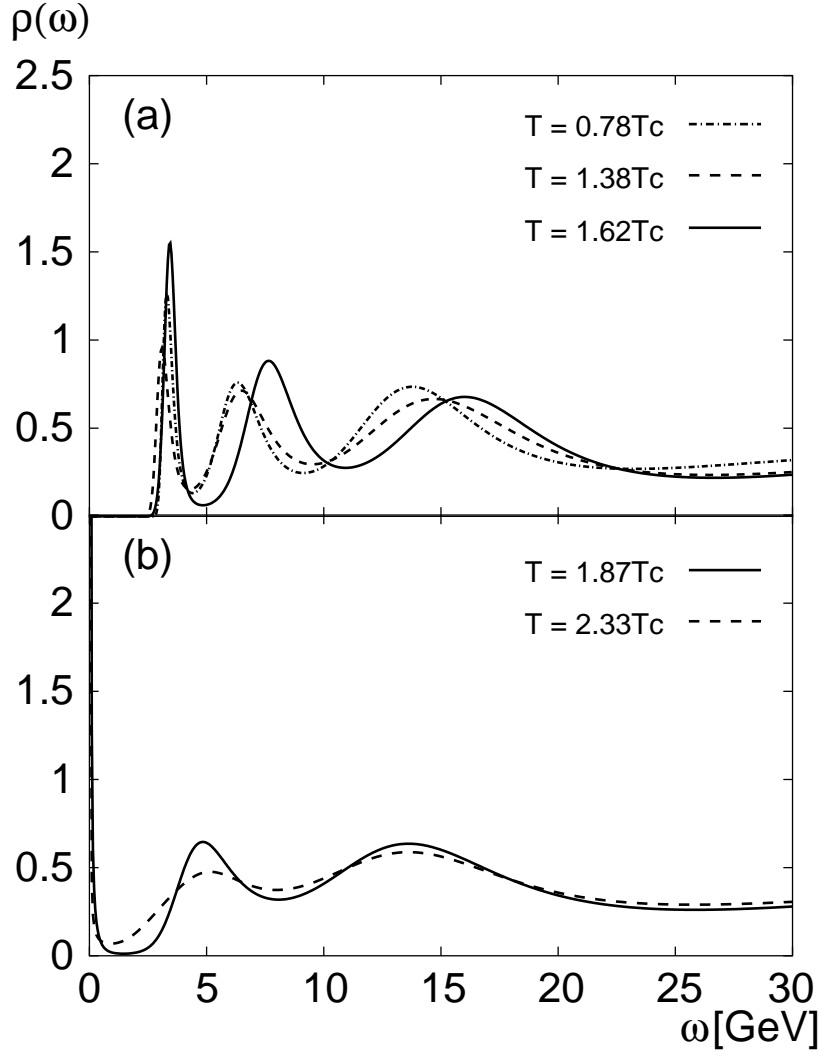


FIG. 30: Spectral density  $\rho(\omega)$  for the  $J/\psi$  for several temperatures shown in units of the crossover temperature  $T_c$  [128]. The ground state peak is visible up to  $1.62T_c$ . These results are obtained in a quenched simulation.

Computing the viscosity has been a well known challenging problem since it was first attempted by Karsch and Wyld [142]. The correlator is noisy, requiring high statistics. As with the  $J/\psi$  correlator, this is a difficult inverse problem. A further complication is that the spectral function has a nasty  $T$ -independent, large  $\omega$ , ultraviolet behavior  $\rho \sim \omega^4$ , which tends to overwhelm the low-frequency contribution to  $C(x, \tau)$  for low  $x_0$ .

Possible remedies include (1) assuming a functional form for  $\rho$  and fitting its parameters [142], (2) decreasing the time interval  $a_t$ , allowing a larger  $N_\tau$  [143], and (3) adding further constraints

on  $\rho$ , such as maximum entropy [144], and working at small nonzero momentum[145].

Meyer [146, 147, 148] has done a new high-statistics calculation in pure Yang-Mills theory and uses a parameterization of the spectral function in terms of an optimized basis set that folds in appropriate perturbative behavior at large  $\omega$  and then emphasizes deviations from this behavior. For the ratio of shear viscosity to entropy density, he finds  $\eta/s = 0.134(33)$  at  $1.65T_c$  where perturbation theory gives 0.8, and for the ratio of bulk viscosity to entropy density,  $\zeta/s < 0.15$  at  $1.65T_c$  and  $\zeta/s < 0.015$  at  $3.2T_c$ . These results support the notion that the plasma is a nearly perfect fluid.

## B. Dilepton emission and related quantities

The dilepton emission rate, the soft photon emissivity, and the electrical conductivity of the plasma are other important transport properties. They are obtained from the thermal correlator of the electric current

$$G_{EM}(x_0, \mathbf{x}, T) = \langle J_\mu(x_0, \mathbf{x}) J_\mu(0) \rangle. \quad (104)$$

$$G_{EM}(x_0, \mathbf{q}, T) = \int_0^\infty \frac{d\omega}{2\pi} K(\omega, x_0, T) \rho_{EM}(\omega, \mathbf{q}, T), \quad (105)$$

Again, this is a difficult inverse problem. The ultraviolet divergence is milder here than with the spectral function of the stress-energy tensor. In this case  $\rho \sim \omega^2$ . Otherwise, the same methods have been applied.

The spectral density  $\rho_{EM}(\omega, 0, T)$  determines the differential dilepton pair production rate [149]:

$$\left. \frac{dW^4}{d\omega d^3p} \right|_{\vec{p}=0} = \frac{5\alpha_{rmem}^2}{27\pi^2} \frac{1}{\omega^2(e^{\omega/T} - 1)} \rho_{EM}(\omega, 0, T). \quad (106)$$

An example of the relationship between the MEM determination of the spectral function and the resulting dilepton rate is given by Karsch *et al.* [150] in Fig. 31. These results show a strong enhancement over the free quark-antiquark pair contribution, at least up to three times  $T_c$  resulting from a vector meson resonance. The hard dilepton rate is obtained from the spectral function for  $\omega/T \gg 1$ , and there is rough agreement between perturbation theory and lattice simulation.

As with the shear and bulk viscosity, the challenge is getting to low frequency to obtain the soft photon emissivity, and at zero frequency, the electrical conductivity:

$$\sigma(T) = \frac{1}{16} \left. \frac{\partial}{\partial \omega} \rho_{EM}(\omega, \mathbf{0}, T) \right|_{\omega=0}, \quad (107)$$

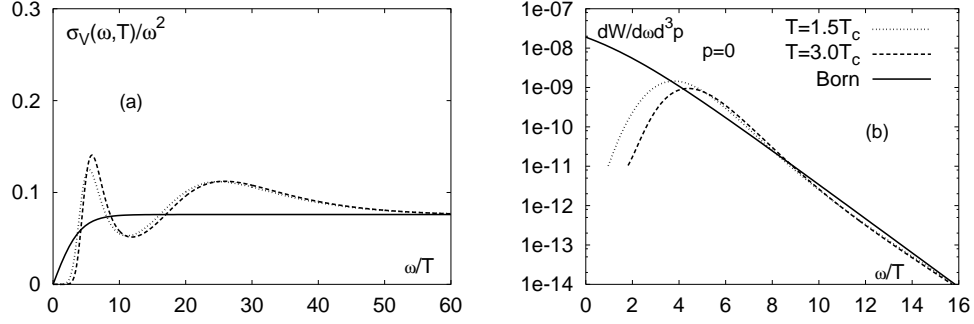


FIG. 31: Relationship between (a) the vector meson spectral density  $\rho_{EM}(\omega, 0, T)$  (shown here as  $\sigma_V(\omega, T)$ ) and (b) the dilepton differential production rate  $dW/d\omega d^3p$  at zero three-momentum, plotted as a function of energy  $\omega$  in units of temperature for two temperatures above the crossover temperature  $T_c$  [150]. The solid lines represent a free quark-antiquark pair. The dash-dotted lines are lattice MEM results that show a peak corresponding to a vector meson resonance. Results are obtained in the quenched approximation.

Extracting the spectral function itself is challenging enough. Extracting its derivative compounds the difficulty. Gupta *et al.* [151] tried different Bayesian priors to constrain the spectral function.

## IX. OUTLOOK

Numerical simulations have taught us much about the properties of high temperature strongly interacting matter. Here are highlights discussed in this article:

- We have a fair understanding of the QCD phase diagram at nonzero temperature and zero or small baryon densities and nearly physical quark masses.
- We have a phenomenologically useful determination of the equation of state.
- We have a good understanding of the behavior of the quark number susceptibility.
- We are beginning to understand the small mass limit of the chiral condensate and its related susceptibilities.
- We know the plasma has persistent confining properties that are observable in screening masses and the spatial string tension.
- We have some indications of the persistence of hadronic states as resonances in the plasma phase at temperatures close to and above  $T_c$ .



- We are starting to determine plasma transport coefficients.
- We are starting to make contact with perturbation theory at high temperatures.

There are many outstanding questions. Here are particularly pressing ones:

- We need a more robust determination of transport coefficients.
- We don't have a good way to simulate at moderately large or higher nonzero baryon number densities.
- We don't know, yet, whether the critical point in the  $\mu/T - T$  plane is experimentally accessible.
- We don't know whether the tricritical point in the  $m_s, m_{u,d}$  plane lies above or below the physical  $m_s$ .
- We would like to understand better the behavior of the equation of state in the region where it overlaps with hadron resonance gas models.
- It would be good to develop more confidence in our understanding of the continuum limit of phenomenologically important quantities.
- It would be good to have high precision results from fermion formulations other than staggered for purposes of corroboration.
- We would like to develop more confidence in our contact with perturbation theory at high temperatures.

Work currently underway will help resolve some of these issues. At zero or small baryon number densities we expect progress with Wilson quark formulations, including clover-improved and twisted-mass. Simulations with domain-wall quarks will help test conclusions about chiral properties. Forthcoming simulations with highly improved staggered quarks (HISQ) will help reduce some of the lattice artifacts of the staggered fermion formulation, especially at temperatures leading up to  $T_c$ , where we suspect they are important.

For simulations at nonzero baryon number densities we really need some new ideas. Perhaps stochastic quantization will help. For transport coefficients and the small-quark-mass region of the phase diagram, we may expect progress simply by applying more computing power.

Lattice QCD thermodynamics is a very active field. We expect continued strong progress in the years to come.

### Acknowledgments

We thank Ludmila Levkova for a careful reading of the manuscript. This work is supported by the National Science Foundation under grants PHY04-56691 and PHY07-57333.

- 
- [1] A. Bazavov *et al.*, *Full nonperturbative QCD simulations with 2+1 flavors of improved staggered quarks*, arXiv: 0903.3598.
  - [2] F. Wilczek, *QCD in extreme conditions*, arXiv: hep-ph/0003183.
  - [3] R. P. Feynman and A. R. Hibbs, *Quantum mechanics and path integrals*. McGraw-Hill, New York, 1965.
  - [4] I. Montvay and G. Münster, *Quantum fields on the computer*. Cambridge Univ. Press, Cambridge, 1997.
  - [5] M. Creutz, *Quantum fields on the computer*. World Scientific, Singapore, 1992.
  - [6] T. DeGrand and C. DeTar, *Lattice methods for quantum chromodynamics*. World Scientific, Singapore, 2006.
  - [7] K. G. Wilson, *Confinement of quarks*, *Phys. Rev.* **D10** (1974) 2445–2459.
  - [8] A. M. Wegner, *Duality in generalized Ising models and phase transitions without local order parameters*, *J. Math. Phys.* **12** (1971) 2259–2272.
  - [9] A. M. Polyakov, *Compact gauge fields and the infrared catastrophe*, *Phys. Lett.* **B59** (1975) 82–84.
  - [10] M. Lüscher and P. Weisz, *On-Shell Improved Lattice Gauge Theories*, *Commun. Math. Phys.* **97** (1985) 59.
  - [11] M. Lüscher and P. Weisz, *Computation of the Action for On-Shell Improved Lattice Gauge Theories at Weak Coupling*, *Phys. Lett.* **B158** (1985) 250.
  - [12] K. Symanzik, *Continuum Limit and Improved Action in Lattice Theories. 2. O(N) Nonlinear Sigma Model in Perturbation Theory*, *Nucl. Phys.* **B226** (1983) 205.
  - [13] B. Sheikholeslami and R. Wohlert, *Improved Continuum Limit Lattice Action for QCD with Wilson Fermions*, *Nucl. Phys.* **B259** (1985) 572.

- [14] **Alpha** Collaboration, R. Frezzotti, P. A. Grassi, S. Sint, and P. Weisz, *Lattice QCD with a chirally twisted mass term*, *JHEP* **08** (2001) 058, [arXiv: hep-lat/0101001].
- [15] R. Frezzotti and G. C. Rossi, *Chirally improving Wilson fermions. I:  $O(a)$  improvement*, *JHEP* **08** (2004) 007, [arXiv: hep-lat/0306014].
- [16] **CP-PACS** Collaboration, A. Ali Khan *et al.*, *Phase structure and critical temperature of two flavor QCD with renormalization group improved gauge action and clover improved Wilson quark action*, *Phys. Rev.* **D63** (2001) 034502, [arXiv: hep-lat/0008011].
- [17] S. Ejiri, *Lattice QCD thermodynamics with Wilson quarks*, *Prog. Theor. Phys. Suppl.* **168** (2007) 245–252, [arXiv: 0704.3747].
- [18] **HPQCD** Collaboration, E. Follana, A. Hart, C. T. H. Davies, and Q. Mason, *The low-lying Dirac spectrum of staggered quarks*, *Phys. Rev.* **D72** (2005) 054501, [arXiv: hep-lat/0507011].
- [19] S. R. Sharpe, *Rooted staggered fermions: Good, bad or ugly?*, *PoS LAT2006* (2006) 022, [arXiv: hep-lat/0610094].
- [20] P. Lepage, *Perturbative improvement for lattice QCD: An update*, *Nucl. Phys. Proc. Suppl.* **60B** (1998) 267–278, [arXiv: hep-lat/9707026].
- [21] **MILC** Collaboration, C. W. Bernard *et al.*, *Quenched hadron spectroscopy with improved staggered quark action*, *Phys. Rev.* **D58** (1998) 014503, [arXiv: hep-lat/9712010].
- [22] J. F. Lagae and D. K. Sinclair, *Improving the staggered quark action to reduce flavour symmetry violations*, *Nucl. Phys. Proc. Suppl.* **63** (1998) 892–894, [arXiv: hep-lat/9709035].
- [23] J. F. Lagae and D. K. Sinclair, *Improved staggered quark actions with reduced flavour symmetry violations for lattice QCD*, *Phys. Rev.* **D59** (1999) 014511, [arXiv: hep-lat/9806014].
- [24] **MILC** Collaboration, K. Orginos and D. Toussaint, *Testing improved actions for dynamical Kogut-Susskind quarks*, *Phys. Rev.* **D59** (1999) 014501, [arXiv: hep-lat/9805009].
- [25] **MILC** Collaboration, D. Toussaint and K. Orginos, *Tests of improved Kogut-Susskind fermion actions*, *Nucl. Phys. Proc. Suppl.* **73** (1999) 909–911, [arXiv: hep-lat/9809148].
- [26] G. P. Lepage, *Flavor-symmetry restoration and Symanzik improvement for staggered quarks*, *Phys. Rev.* **D59** (1999) 074502, [arXiv: hep-lat/9809157].
- [27] **MILC** Collaboration, K. Orginos, D. Toussaint, and R. L. Sugar, *Variants of fattening and flavor symmetry restoration*, *Phys. Rev.* **D60** (1999) 054503, [arXiv: hep-lat/9903032].
- [28] **MILC** Collaboration, C. W. Bernard *et al.*, *Scaling tests of the improved Kogut-Susskind quark action*, *Phys. Rev.* **D61** (2000) 111502, [arXiv: hep-lat/9912018].

- [29] U. M. Heller, F. Karsch, and B. Sturm, *Improved staggered fermion actions for QCD thermodynamics*, *Phys. Rev.* **D60** (1999) 114502, [arXiv: hep-lat/9901010].
- [30] F. Karsch, E. Laermann, and A. Peikert, *The pressure in 2, 2+1 and 3 flavour QCD*, *Phys. Lett.* **B478** (2000) 447–455, [arXiv: hep-lat/0002003].
- [31] **HPQCD** Collaboration, E. Follana *et al.*, *Highly improved staggered quarks on the lattice, with applications to charm physics*, *Phys. Rev.* **D75** (2007) 054502, [arXiv: hep-lat/0610092].
- [32] Y. Aoki, Z. Fodor, S. D. Katz, and K. K. Szabó, *The QCD transition temperature: Results with physical masses in the continuum limit*, *Phys. Lett.* **B643** (2006) 46–54, [arXiv: hep-lat/0609068].
- [33] N. Ishizuka, M. Fukugita, H. Mino, M. Okawa, and A. Ukawa, *Operator dependence of hadron masses for Kogut-Susskind quarks on the lattice*, *Nucl. Phys.* **B411** (1994) 875–902.
- [34] D. B. Kaplan, *A Method for simulating chiral fermions on the lattice*, *Phys. Lett.* **B288** (1992) 342–347, [arXiv: hep-lat/9206013].
- [35] V. Furman and Y. Shamir, *Axial symmetries in lattice QCD with Kaplan fermions*, *Nucl. Phys.* **B439** (1995) 54–78, [arXiv: hep-lat/9405004].
- [36] R. G. Edwards, U. M. Heller, and R. Narayanan, *Spectral flow, chiral condensate and topology in lattice QCD*, *Nucl. Phys.* **B535** (1998) 403–422, [arXiv: hep-lat/9802016].
- [37] M. Golterman, Y. Shamir, and B. Svetitsky, *Localization properties of lattice fermions with plaquette and improved gauge actions*, *Phys. Rev.* **D72** (2005) 034501, [arXiv: hep-lat/0503037].
- [38] **RBC** Collaboration, D. J. Antonio *et al.*, *Localization and chiral symmetry in 3 flavor domain wall QCD*, *Phys. Rev.* **D77** (2008) 014509, [arXiv: 0705.2340].
- [39] P. Chen *et al.*, *The finite temperature QCD phase transition with domain wall fermions*, *Phys. Rev.* **D64** (2001) 014503, [arXiv: hep-lat/0006010].
- [40] **RBC-HotQCD** Collaboration, M. Cheng, *QCD Thermodynamics with Domain Wall Fermions*, *PoS LAT2008* (2008) 180, [arXiv: 0810.1311].
- [41] R. Narayanan and H. Neuberger, *A Construction of lattice chiral gauge theories*, *Nucl. Phys.* **B443** (1995) 305–385, [arXiv: hep-th/9411108].
- [42] H. Neuberger, *Exactly massless quarks on the lattice*, *Phys. Lett.* **B417** (1998) 141–144, [arXiv: hep-lat/9707022].
- [43] P. H. Ginsparg and K. G. Wilson, *A Remnant of Chiral Symmetry on the Lattice*, *Phys. Rev.* **D25** (1982) 2649.
- [44] M. Lüscher, *Exact chiral symmetry on the lattice and the Ginsparg- Wilson relation*, *Phys. Lett.*

- B428** (1998) 342–345, [arXiv: hep-lat/9802011].
- [45] Z. Fodor, S. D. Katz, and K. K. Szabó, *Dynamical overlap fermions, results with hybrid Monte-Carlo algorithm*, *JHEP* **08** (2004) 003, [arXiv: hep-lat/0311010].
- [46] P. Hegde, F. Karsch, E. Laermann, and S. Shcheredin, *Lattice cut-off effects and their reduction in studies of QCD thermodynamics at non-zero temperature and chemical potential*, *Eur. Phys. J.* **C55** (2008) 423–437, [arXiv: 0801.4883].
- [47] W. Bietenholz, R. Brower, S. Chandrasekharan, and U. J. Wiese, *Progress on perfect lattice actions for QCD*, *Nucl. Phys. Proc. Suppl.* **53** (1997) 921–934, [arXiv: hep-lat/9608068].
- [48] R. Sommer, *A New way to set the energy scale in lattice gauge theories and its applications to the static force and alpha-s in SU(2) Yang-Mills theory*, *Nucl. Phys.* **B411** (1994) 839–854, [arXiv: hep-lat/9310022].
- [49] R. Gupta *et al.*, *The EOS from simulations on BlueGene L Supercomputer at LLNL and NYBlue*, *PoS LAT2008* (2008) 170.
- [50] **HotQCD** Collaboration, C. DeTar and R. Gupta, *Toward a precise determination of  $T_c$  with 2+1 flavors of quarks*, *PoS LAT2007* (2007) 179, [arXiv: 0710.1655].
- [51] **HotQCD** Collaboration, A. Bazavov *et al.*, *Equation of state and QCD transition at finite temperature*, arXiv: 0903.4379.
- [52] **MILC** Collaboration, C. Bernard *et al.*, *QCD thermodynamics with three flavors of improved staggered quarks*, *Phys. Rev.* **D71** (2005) 034504, [arXiv: hep-lat/0405029].
- [53] M. Peskin and D. V. Schroeder, *An Introduction to Quantum Field Theory*. Westview Press, New York, 1995.
- [54] **RBC-Bielefeld** Collaboration, F. Karsch, *Fluctuations of Goldstone modes and the chiral transition in QCD*, *Nucl. Phys.* **A820** (2008) 99C–102C, [arXiv: 0810.3078].
- [55] Y. Maezawa *et al.*, *Thermodynamics and heavy-quark free energies at finite temperature and density with two flavors of improved Wilson quarks*, *PoS LAT2007* (2007) 207, [arXiv: 0710.0945].
- [56] W. Soeldner, *Quark Mass Dependence of the QCD Equation of State on  $N_t=8$  Lattices*, *PoS LAT2008* (2008) 173.
- [57] Y. Aoki *et al.*, *The QCD transition temperature: results with physical masses in the continuum limit II*, arXiv: 0903.4155.
- [58] **MILC** Collaboration, C. Aubin *et al.*, *Light hadrons with improved staggered quarks: Approaching the continuum limit*, *Phys. Rev.* **D70** (2004) 094505, [arXiv: hep-lat/0402030].

- [59] G. Boyd *et al.*, *Equation of state for the SU(3) gauge theory*, *Phys. Rev. Lett.* **75** (1995) 4169–4172, [arXiv: hep-lat/9506025].
- [60] R. D. Pisarski and F. Wilczek, *Remarks on the Chiral Phase Transition in Chromodynamics*, *Phys. Rev.* **D29** (1984) 338–341.
- [61] F. Karsch, E. Laermann, and C. Schmidt, *The chiral critical point in 3-flavor QCD*, *Phys. Lett.* **B520** (2001) 41–49, [arXiv: hep-lat/0107020].
- [62] F. Karsch *et al.*, *Where is the chiral critical point in 3-flavor QCD?*, *Nucl. Phys. Proc. Suppl.* **129** (2004) 614–616, [arXiv: hep-lat/0309116].
- [63] E. Laermann and O. Philipsen, *Status of lattice QCD at finite temperature*, *Ann. Rev. Nucl. Part. Sci.* **53** (2003) 163–198, [arXiv: hep-ph/0303042].
- [64] P. de Forcrand and O. Philipsen, *The chiral critical line of  $N(f) = 2+1$  QCD at zero and non-zero baryon density*, *JHEP* **01** (2007) 077, [arXiv: hep-lat/0607017].
- [65] Y. Aoki, G. Endrödi, Z. Fodor, S. D. Katz, and K. K. Szabó, *The order of the quantum chromodynamics transition predicted by the standard model of particle physics*, *Nature* **443** (2006) 675–678, [arXiv: hep-lat/0611014].
- [66] T. Mendes, *Universality and Scaling at the chiral transition in two-flavor QCD at finite temperature*, *PoS LAT2007* (2007) 208, [arXiv: 0710.0746].
- [67] J. B. Kogut and D. K. Sinclair, *Evidence for  $O(2)$  universality at the finite temperature transition for lattice QCD with 2 flavours of massless staggered quarks*, *Phys. Rev.* **D73** (2006) 074512, [arXiv: hep-lat/0603021].
- [68] M. D’Elia, A. Di Giacomo, and C. Pica, *Two flavor QCD and confinement*, *Phys. Rev.* **D72** (2005) 114510, [arXiv: hep-lat/0503030].
- [69] A. M. Halasz, A. D. Jackson, R. E. Shrock, M. A. Stephanov, and J. J. M. Verbaarschot, *On the phase diagram of QCD*, *Phys. Rev.* **D58** (1998) 096007, [arXiv: hep-ph/9804290].
- [70] J. B. Kogut *et al.*, *Chiral Symmetry Restoration in Baryon Rich Environments*, *Nucl. Phys.* **B225** (1983) 93.
- [71] F. Karsch, *Lattice simulations of the thermodynamics of strongly interacting elementary particles and the exploration of new phases of matter in relativistic heavy ion collisions*, *J. Phys. Conf. Ser.* **46** (2006) 122–131, [arXiv: hep-lat/0608003].
- [72] M. G. Alford, K. Rajagopal, and F. Wilczek, *Color-flavor locking and chiral symmetry breaking in high density QCD*, *Nucl. Phys.* **B537** (1999) 443–458, [arXiv: hep-ph/9804403].

- [73] R. Rapp, T. Schafer, E. V. Shuryak, and M. Velkovsky, *Diquark Bose condensates in high density matter and instantons*, *Phys. Rev. Lett.* **81** (1998) 53–56, [arXiv: hep-ph/9711396].
- [74] M. Golterman, Y. Shamir, and B. Svetitsky, *Breakdown of staggered fermions at nonzero chemical potential*, *Phys. Rev.* **D74** (2006) 071501, [arXiv: hep-lat/0602026].
- [75] O. Philipsen, *The QCD phase diagram at zero and small baryon density*, *PoS LAT2005* (2006) 016, [arXiv: hep-lat/0510077].
- [76] S. Ejiri, *Recent progress in lattice QCD at finite density*, *PoS LAT2008* (2008) 002.
- [77] A. M. Ferrenberg and R. H. Swendsen, *New Monte Carlo Technique for Studying Phase Transitions*, *Phys. Rev. Lett.* **61** (1988) 2635–2638.
- [78] A. M. Ferrenberg and R. H. Swendsen, *Optimized Monte Carlo analysis*, *Phys. Rev. Lett.* **63** (1989) 1195–1198.
- [79] D. Toussaint, *Simulating QCD at finite density*, *Nucl. Phys. Proc. Suppl.* **17** (1990) 248–251.
- [80] Z. Fodor and S. D. Katz, *A new method to study lattice QCD at finite temperature and chemical potential*, *Phys. Lett.* **B534** (2002) 87–92, [arXiv: hep-lat/0104001].
- [81] Z. Fodor and S. D. Katz, *Critical point of QCD at finite  $T$  and  $\mu$ , lattice results for physical quark masses*, *JHEP* **04** (2004) 050, [arXiv: hep-lat/0402006].
- [82] Z. Fodor and S. D. Katz, *Lattice determination of the critical point of QCD at finite  $T$  and  $\mu$* , *JHEP* **03** (2002) 014, [arXiv: hep-lat/0106002].
- [83] J. B. Kogut and D. K. Sinclair, *Lattice QCD at finite isospin density at zero and finite temperature*, *Phys. Rev.* **D66** (2002) 034505, [arXiv: hep-lat/0202028].
- [84] J. B. Kogut and D. K. Sinclair, *Lattice QCD at finite temperature and density in the phase-quenched approximation*, *Phys. Rev.* **D77** (2008) 114503, [arXiv: 0712.2625].
- [85] P. de Forcrand, M. A. Stephanov, and U. Wenger, *On the phase diagram of QCD at finite isospin density*, *PoS LAT2007* (2007) 237, [arXiv: 0711.0023].
- [86] I. M. Barbour, S. E. Morrison, E. G. Klepfish, J. B. Kogut, and M.-P. Lombardo, *Results on finite density QCD*, *Nucl. Phys. Proc. Suppl.* **60B** (1998) 220–234, [arXiv: hep-lat/9705042].
- [87] J. Engels, O. Kaczmarek, F. Karsch, and E. Laermann, *The quenched limit of lattice QCD at non-zero baryon number*, *Nucl. Phys.* **B558** (1999) 307–326, [arXiv: hep-lat/9903030].
- [88] P. de Forcrand and S. Kratochvila, *Finite density QCD with a canonical approach*, *Nucl. Phys. Proc. Suppl.* **153** (2006) 62–67, [arXiv: hep-lat/0602024].
- [89] A. Alexandru, M. Faber, I. Horvath, and K.-F. Liu, *Lattice QCD at finite density via a new*

- canonical approach*, *Phys. Rev.* **D72** (2005) 114513, [arXiv: hep-lat/0507020].
- [90] X.-f. Meng, A. Li, A. Alexandru, and K.-F. Liu, *Winding number expansion for the canonical approach to finite density simulations*, *PoS LATTICE2008* (2008) 032, [arXiv: 0811.2112].
- [91] A. Li, X. Meng, A. Alexandru, and K.-F. Liu, *Finite Density Simulations with Canonical Ensemble*, *PoS LATTICE2008* (2008) 178, [arXiv: 0810.2349].
- [92] P. de Forcrand and O. Philipsen, *The QCD phase diagram for small densities from imaginary chemical potential*, *Nucl. Phys.* **B642** (2002) 290–306, [arXiv: hep-lat/0205016].
- [93] M. D’Elia and M.-P. Lombardo, *Finite density QCD via imaginary chemical potential*, *Phys. Rev.* **D67** (2003) 014505, [arXiv: hep-lat/0209146].
- [94] C. R. Allton *et al.*, *The QCD thermal phase transition in the presence of a small chemical potential*, *Phys. Rev.* **D66** (2002) 074507, [arXiv: hep-lat/0204010].
- [95] R. V. Gavai and S. Gupta, *Pressure and non-linear susceptibilities in QCD at finite chemical potentials*, *Phys. Rev.* **D68** (2003) 034506, [arXiv: hep-lat/0303013].
- [96] R. V. Gavai and S. Gupta, *The critical end point of QCD*, *Phys. Rev.* **D71** (2005) 114014, [arXiv: hep-lat/0412035].
- [97] R. V. Gavai and S. Gupta, *QCD at finite chemical potential with six time slices*, *Phys. Rev.* **D78** (2008) 114503, [arXiv: 0806.2233].
- [98] Z. Fodor, S. D. Katz, and C. Schmidt, *The density of states method at non-zero chemical potential*, *JHEP* **03** (2007) 121, [arXiv: hep-lat/0701022].
- [99] S. Ejiri, *On the existence of the critical point in finite density lattice QCD*, *Phys. Rev.* **D77** (2008) 014508, [arXiv: 0706.3549].
- [100] G. Aarts and I.-O. Stamatescu, *Stochastic quantization at finite chemical potential*, *JHEP* **09** (2008) 018, [arXiv: 0807.1597].
- [101] G. Parisi and Y.-s. Wu, *Perturbation Theory Without Gauge Fixing*, *Sci. Sin.* **24** (1981) 483.
- [102] G. Parisi, *On complex probabilities*, *Phys. Lett.* **B131** (1983) 393–395.
- [103] P. H. Damgaard and H. Hüffel, *Stochastic Quantization*, *Phys. Rept.* **152** (1987) 227.
- [104] G. Aarts, *Can stochastic quantization evade the sign problem? – the relativistic Bose gas at finite chemical potential*, *Phys. Rev. Lett.* **102** (2009) 131601, [arXiv: 0810.2089].
- [105] G. Aarts, *Complex Langevin dynamics at finite chemical potential: mean field analysis in the relativistic Bose gas*, *JHEP* **05** (2009) 052, [arXiv: 0902.4686].
- [106] P. de Forcrand, S. Kim, and O. Philipsen, *A QCD chiral critical point at small chemical potential: is*



- it there or not?*, *PoS LAT2007* (2007) 178, [arXiv: 0711.0262].
- [107] P. de Forcrand and O. Philipsen, *The curvature of the critical surface  $(m_u, d, m_s)^{crit}(\mu)$ : a progress report*, *PoS LATTICE2008* (2008) 208, [arXiv: 0811.3858].
- [108] P. de Forcrand and O. Philipsen, *The chiral critical point of  $N_f=3$  QCD at finite density to the order  $(\mu/T)^4$* , *JHEP* **11** (2008) 012, [arXiv: 0808.1096].
- [109] J. Engels, J. Fingberg, F. Karsch, D. Miller, and M. Weber, *Nonperturbative thermodynamics of  $SU(N)$  gauge theories*, *Phys. Lett.* **B252** (1990) 625–630.
- [110] P. Petreczky, *Quark Matter 2009: Finite temperature lattice QCD: Present status*, .
- [111] M. Laine and Y. Schröder, *Quark mass thresholds in QCD thermodynamics*, *Phys. Rev.* **D73** (2006) 085009, [arXiv: hep-ph/0603048].
- [112] **CP-PACS** Collaboration, A. Ali Khan *et al.*, *Equation of state in finite-temperature QCD with two flavors of improved Wilson quarks*, *Phys. Rev.* **D64** (2001) 074510, [arXiv: hep-lat/0103028].
- [113] T. Umeda *et al.*, *Fixed Scale Approach to Equation of State in Lattice QCD*, *Phys. Rev.* **D79** (2009) 051501, [arXiv: 0809.2842].
- [114] L. Levkova, T. Manke, and R. Mawhinney, *Two-flavor QCD thermodynamics using anisotropic lattices*, *Phys. Rev.* **D73** (2006) 074504, [arXiv: hep-lat/0603031].
- [115] T. Umeda *et al.*, *Thermodynamics of  $SU(3)$  gauge theory at fixed lattice spacing*, *PoS LAT2008* (2008) 174.
- [116] G. Endrödi, Z. Fodor, S. D. Katz, and K. K. Szabó, *The equation of state at high temperatures from lattice QCD*, *PoS LAT2007* (2007) 228, [arXiv: 0710.4197].
- [117] E. Braaten and A. Nieto, *Free Energy of QCD at High Temperature*, *Phys. Rev.* **D53** (1996) 3421–3437, [arXiv: hep-ph/9510408].
- [118] K. Kajantie, M. Laine, K. Rummukainen, and Y. Schröder, *The pressure of hot QCD up to  $g^{**6} \ln(1/g)$* , *Phys. Rev.* **D67** (2003) 105008, [arXiv: hep-ph/0211321].
- [119] G. Boyd *et al.*, *Thermodynamics of  $SU(3)$  Lattice Gauge Theory*, *Nucl. Phys.* **B469** (1996) 419–444, [arXiv: hep-lat/9602007].
- [120] **MILC** Collaboration, C. Bernard *et al.*, *QCD thermodynamics with 2+1 flavors at nonzero chemical potential*, *Phys. Rev.* **D77** (2008) 014503, [arXiv: 0710.1330].
- [121] **MILC** Collaboration, S. Basak *et al.*, *QCD equation of state at non-zero chemical potential*, *PoS LAT2008* (2008) 171.
- [122] P. H. Ginsparg, *First Order and Second Order Phase Transitions in Gauge Theories at Finite*

- Temperature, Nucl. Phys.* **B170** (1980) 388.
- [123] T. Appelquist and R. D. Pisarski, *High-Temperature Yang-Mills Theories and Three-Dimensional Quantum Chromodynamics*, *Phys. Rev.* **D23** (1981) 2305.
- [124] M. Cheng *et al.*, *The Spatial String Tension and Dimensional Reduction in QCD*, *Phys. Rev.* **D78** (2008) 034506, [arXiv: 0806.3264].
- [125] C. E. DeTar, *A Conjecture Concerning the Modes of Excitation of the Quark-Gluon Plasma*, *Phys. Rev.* **D32** (1985) 276.
- [126] M. Cheng *et al.*, *The QCD Equation of State with almost Physical Quark Masses*, *Phys. Rev.* **D77** (2008) 014511, [arXiv: 0710.0354].
- [127] E. Laermann *et al.*, *Recent results on screening masses*, *PoS LAT2008* (2008) 193.
- [128] M. Asakawa and T. Hatsuda, *J/psi and eta/c in the deconfined plasma from lattice QCD*, *Phys. Rev. Lett.* **92** (2004) 012001, [arXiv: hep-lat/0308034].
- [129] S. Datta, F. Karsch, P. Petreczky, and I. Wetzorke, *Behavior of charmonium systems after deconfinement*, *Phys. Rev.* **D69** (2004) 094507, [arXiv: hep-lat/0312037].
- [130] T. Matsui and H. Satz, *J/psi Suppression by Quark-Gluon Plasma Formation*, *Phys. Lett.* **B178** (1986) 416.
- [131] O. Jahn and O. Philipsen, *The Polyakov loop and its relation to static quark potentials and free energies*, *Phys. Rev.* **D70** (2004) 074504, [arXiv: hep-lat/0407042].
- [132] A. Mocsy and P. Petreczky, *Can quarkonia survive deconfinement ?*, *Phys. Rev.* **D77** (2008) 014501, [arXiv: 0705.2559].
- [133] M. Laine, O. Philipsen, P. Romatschke, and M. Tassler, *Real-time static potential in hot QCD*, *JHEP* **03** (2007) 054, [arXiv: hep-ph/0611300].
- [134] M. A. Escobedo and J. Soto, *Non-relativistic bound states at finite temperature (I): the hydrogen atom*, *Phys. Rev. A* **78** (2008) 032520, [arXiv: 0804.0691].
- [135] N. Brambilla, J. Ghiglieri, A. Vairo, and P. Petreczky, *Static quark-antiquark pairs at finite temperature*, *Phys. Rev.* **D78** (2008) 014017, [arXiv: 0804.0993].
- [136] T. Umeda, K. Nomura, and H. Matsufuru, *Charmonium at finite temperature in quenched lattice QCD*, *Eur. Phys. J.* **C39S1** (2005) 9–26, [arXiv: hep-lat/0211003].
- [137] M. Jarrell and J. Gubernatis, *Bayesian inference and the analytic continuation of imaginary-time quantum Monte Carlo data*, *Phys. Rep.* **269** (1996) 133.
- [138] Y. Nakahara, M. Asakawa, and T. Hatsuda, *Hadronic spectral functions in lattice QCD*, *Phys. Rev.*

- D60** (1999) 091503, [arXiv: hep-lat/9905034].
- [139] M. Asakawa, T. Hatsuda, and Y. Nakahara, *Maximum entropy analysis of the spectral functions in lattice QCD*, *Prog. Part. Nucl. Phys.* **46** (2001) 459–508, [arXiv: hep-lat/0011040].
- [140] G. Aarts, C. Allton, M. B. Oktay, M. Peardon, and J.-I. Skullerud, *Charmonium at high temperature in two-flavor QCD*, *Phys. Rev.* **D76** (2007) 094513, [arXiv: 0705.2198].
- [141] H. T. Ding, O. Kaczmarek, F. Karsch, and H. Satz, *Charmonium correlators and spectral functions at finite temperature*, *PoS CONFINEMENT8* (2008) 108, [arXiv: 0901.3023].
- [142] F. Karsch and H. W. Wyld, *Thermal Green's functions and transport coefficients on the lattice*, *Phys. Rev.* **D35** (1987) 2518.
- [143] G. Burgers, F. Karsch, A. Nakamura, and I. O. Stamatescu, *QCD on anisotropic lattices*, *Nucl. Phys.* **B304** (1988) 587.
- [144] G. Aarts, C. Allton, J. Foley, S. Hands, and S. Kim, *Spectral functions at small energies and the electrical conductivity in hot, quenched lattice QCD*, *Phys. Rev. Lett.* **99** (2007) 022002, [arXiv: hep-lat/0703008].
- [145] H. B. Meyer, *Energy-momentum tensor correlators and spectral functions*, *JHEP* **08** (2008) 031, [arXiv: 0806.3914].
- [146] H. Meyer, *Energy-momentum tensor correlators and viscosity*, *PoS LAT2008* (2008) 017.
- [147] H. B. Meyer, *A calculation of the bulk viscosity in SU(3) gluodynamics*, *Phys. Rev. Lett.* **100** (2008) 162001, [arXiv: 0710.3717].
- [148] H. B. Meyer, *A calculation of the shear viscosity in SU(3) gluodynamics*, *Phys. Rev.* **D76** (2007) 101701, [arXiv: 0704.1801].
- [149] E. Braaten, R. D. Pisarski, and T.-C. Yuan, *Production of soft dileptons in the quark - gluon plasma*, *Phys. Rev. Lett.* **64** (1990) 2242.
- [150] F. Karsch, E. Laermann, P. Petreczky, S. Stickan, and I. Wetzorke, *A lattice calculation of thermal dilepton rates*, *Phys. Lett.* **B530** (2002) 147–152, [arXiv: hep-lat/0110208].
- [151] S. Gupta, *The electrical conductivity and soft photon emissivity of the QCD plasma*, *Phys. Lett.* **B597** (2004) 57–62, [arXiv: hep-lat/0301006].